# An Acoustic Indoor Localization System for Unmanned Robots with Temperature Compensation and Co-channel Interference Tolerance

**Tsay Lok Wai Jacky**

**2022**

# An Acoustic Indoor Localization System for Unmanned Robots with Temperature Compensation and Co-channel Interference Tolerance

**Tsay Lok Wai Jacky**


**Division of Environmental Science and Technology**
**Graduate School of Agriculture**
**Kyoto University**

**2022**

# An Acoustic Indoor Localization System for Unmanned Robots with Temperature Compensation and Co-channel Interference Tolerance

**Tsay Lok Wai Jacky**

Dissertation
Submitted in partial fulfillment of the requirements for the degree of doctor in agricultural science

**Division of Environmental Science and Technology**
**Graduate School of Agriculture**
**Kyoto University**

**2022**

# Table of Contents

# List of Figures

# List of Tables

# Chapter 1 Introduction

## 1.1 Background

In recent years, agriculture has seen a sustained effort to improve the technology of field robotics (Bechar and Vigneault, 2016; Vougioukas, 2019). These robots and new precision farming technologies are needed in places like Japan, where the population is aging, and the supply of farm labor is declining (Hayashi et al., 2014). Unmanned robots are necessary in agriculture industry to replace a high demand of farmers and increase the food production efficiency. However, the current situation of the robotic systems are mainly for an outdoor field and very few of these labor replacing robots have been designed and tested for greenhouse operations (Mautz, 2009). Though the existing robotic rail systems have the potential to aid farmers with the monitoring of crops as well as for more efficient work operations in the greenhouse (Kawamura et al., 1984), they have the problems of heavy, expensive and slow operation speed for robots moving along the rails.

To automate agricultural systems, a new concept of Internet of Things (IoT) (Spachos, 2020) that is based on building networks of several devices and sensors has been developed. The proposed new robotic scheme in the greenhouse uses multiple robots including the unmanned ground vehicles (UGV) and unmanned aerial vehicles (UAV). It can overcome the current problems by building a network of small operating robots that UAV can monitor the crops and collect the field data while UGV can perform the fertilizing and harvesting activities. In many cases, these networks require a localization system, which provides localization information of the devices and sensors. With knowing the position of the devices, controlling the movement of the robots becomes possible. Thus, a reliable and accurate indoor localization system is essential for this new concept of greenhouse precision farming.

To date, global navigation satellite systems (GNSS) (Koura et al., 2001; Mercado et al., 2013), laser trackers (Jia et al., 2019), radio frequency identification (RFID) (Shirehjini et al., 2012; Yan and Chu, 2020), Bluetooth low energy (BLE) beacon (Spachos et al., 2018), ultrasound systems (Atri Mandal, 2005; Khyam et al., 2017) and positioning by signal strength (Chan et al., 2009; Huang et al., 2020) have been utilized. However, these systems are not only limited to outdoor uses, but some of them are not accurate enough (Bellone et al., 2016), intolerant of obstacles, very heavy and cannot be installed in a greenhouse (De Preter et al., 2018). The Ultra-Wide Band (UWB), is normally an active structure with around 100 mm accuracy (Delamare et al., 2019; Mazhar et al., 2017) and the accuracy is affected from the signal interference from a broad bandwidth (Nikookar and Prasad, 2009). The indoor performances of these technologies are limited in many aspects, such as low obstacle tolerance, expensive, small coverage area as well as low accuracy.

To overcome these issues, an acoustic-based low-cost and high accuracy method, the spectrum spread sound local positioning system (SSSLPS) is investigated. The system uses a wide band frequency of sound signal which can tolerate both noises and obstacles. There have been some previous researches (Atri Mandal, 2005; Medina et al., 2013; Rishabh et al., 2012) done on evaluating the properties and the accuracy of the acoustic localization systems that can cover a 100 $m^2$ field and provide a centimeter-level accuracy and our research team of the SSSLPS's previous researches were focusing on the orientation, base station and noise tolerance (Huang et al., 2019) etc. The concept of using the spread spectrum sound (SS Sound) enables indoor localization using only relatively inexpensive speakers and microphones. Such a SS Sound system does not require a laser emitter, nor a photodetector to detect the pulse compared with a laser emitter system, and requires less devices compared to an RFID based system. In addition, it does not suffer from the disadvantages of a BLE bacon system, namely, low accuracy and interference with 2.4 GHz devices, etc.

There are still many problems on the road to a fully automated robot system using SSSLPS for controlling multiple robots in a greenhouse. To calculate a range measurement, temperature data is being used to get the sound velocity. Putting temperature sensors at the nodes of speakers and microphones are not enough to estimate the sound velocity of the whole path of signal transmission. A better temperature compensation method can solve the need of temperature sensors and increase the accuracy.

Meanwhile, the signal co-channel interference problem, also known as the signal crosstalk problem, is affecting the effective detection rate of the SSSLPS. Only using the encoding method of SS Sound creates a near-far problem from the similar signal sources of different speakers. It is necessary to evaluate a suitable modulation method for SS Sound. For the problems of dynamic movement of robots, previous research has showed that the noises were mainly from motor (at 6 kHz) and propellers (over 10 kHz) measured by the experiment using a quadcopter with four sets of propellers at different thrust (Intaratep et al., 2016). The conventional Doppler shift compensation that using an extra ultrasound for detecting the frequency shift is not suitable for UAV (Widodo et al., 2013) as the noises are spread over a large frequency bandwidth. A new Doppler compensation algorithm needs to be designed for localizing UAV.

To apply a mature SSSLPS for our concept for future greenhouse automation farming, assignments are to solve temperature compensation problem, signal co-channel interference problem, and the dynamic measurement problem for UGV and UAV.

## 1.2 Research objectives

The objective of this dissertation is to develop a localization system for controlling multiple small ground and aerial robots in the greenhouse. In this paper, SSSLPS is being focused and improved to achieve the objective. To do it, three sub-objectives are being separated.

1. Develop temperature compensation method without using temperature sensor

The main reasons of range errors are inaccurate values of sound velocity or the correlation peak time. Using temperature sensors can only attaining the temperature points of the specific area and it is hard to set so many sensors to get the correct sound velocity for the signal path. Assuming in a closed field that temperature is distributed evenly, the new algorithm is getting a precise estimated sound velocity of the signal path and reducing the need of temperature sensing devices.

2. Evaluate the signal co-channel interference problem

Although SS Sound uses a M-sequence to encode the signal in order to increase the noise tolerance, the signal can still be affected by SS Sound signals sources from other speakers. Finding the correct correlation peak can be difficult when the SSSLPS encounters signal co-channel interference. Evaluation of the signal multiple access methods is essential to determine whether the common frequency division method or time division method is a better option for different situations of the SSSLPS.

3. Develop and evaluate Doppler shift compensation algorithm

The reasons that affecting the dynamic measurement of SSSLPS are acoustic interference by motor or propeller noises and the Doppler shift of the robot moving speed. The hypothesis of the new frequency shift algorithm can tackle the noises by

using more computing power to estimate the change of carrier frequency and chip rate. Giving a correct information of finding the signal's time of arrival and increasing the successful measurement rate.

## 1.3 Dissertation outline

**Chapter 1** introduces the objectives and outline of this research and states the problem of the current SSSLPS.

**Chapter 2** introduces the distance measurement and position estimation by SSSLPS. The hardware device and software program are listed. A compact wireless receiver unit using the Zigbee communication module is introduced.

**Chapter 3** describes the temperature compensation algorithm and tested in a small sized greenhouse. The methods of using temperature sensor (sensor method) and proposed estimated sound velocity method (estimated method) are being compared in a Japanese farmer's greenhouse in Ehime prefecture. The greenhouse effects and the temperature distribution.

**Chapter 4** evaluates the signal co-channel interference and the coverage of SSSLPS in a commercial large sized greenhouse. The properties of SS Sound and the SNR are compared to evaluate the co-channel interference. Finally, an experiment is used to evaluate the dynamic positioning accuracy using SSSLPS for UGV.

**Chapter 5** describes the proposed Doppler shift compensation algorithm for the UAV. The frequency shift algorithm solved the problems of UAV noise interference as well as the changing velocity of UAV. The positioning accuracy is conducted with the Vicon system, which is a machine vision-based positioning system with 0.1 mm accuracy. The

acoustic noise spectrum of the UAV is also evaluated.

**Chapter 6** concludes the objectives achieved and discusses future research topics as well as possible applications for improving the acoustic-based positioning system, SSSLPS.

# Chapter 2 Spread Spectrum Sound-based Local Positioning System

## 2.1 Spread spectrum sound properties

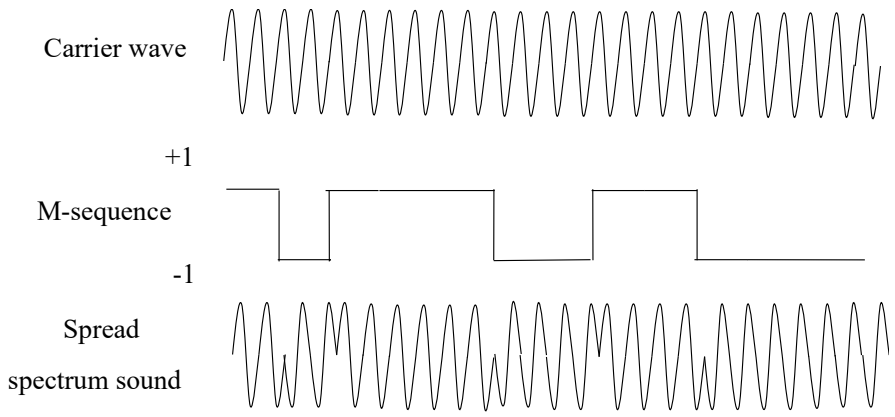


**Fig.2.1** Generation of SS Sound

Fig. 2.1 illustrates the generation of the spread spectrum sound (SS Sound). The sound is encoded by maximal length sequence (M-sequence), which is a pseudo random sequence and has a good autocorrelation performance (Mostafa et al., 2020). The length of the M-sequence was 1023, the chip rate was 12 kcps. Then it was multiplied by a carrier wave of 24 kHz. The frequency of the spread spectrum sound signal is from 12 to 36 kHz. The sampling frequency and sampling bit of the sound signals in the audio interface were 96 kHz and 16 bits, respectively.

At the start of the SS Sound signal package, a trigger signal in an isolated channel is necessary to synchronize the start time of both transmission and reception. After the trigger signal was recognized, the cross-correlation (Huang et al., 2019) value was calculated.

The spread spectrum sound, $s(n)$, was generated by binary phase shift keying

(BPSK) modulating with persuade sequence, as shown in Eq.(1). In this research, M-sequences with 1023 length were used as persuade sequence in four channels. By this modulation, noise tolerance and encoding security were enabled to the positioning system.

$$s(n) = \sin\left[\frac{2\pi f_{cj}(n)}{f_s}\right] \times M\left\{floor\left[\frac{f_{chip}(n)}{f_s}\right]\right\} \quad (1)$$

where $n$ = 0, 1, 2 … 8183 (8183 = sampling frequency / chip rate × M-sequence length - 1), $M$ is vector of M-sequence, $f_{cj}$ [Hz] is carrier frequency of channel $j$, $f_{chip}$ [cps] is chip rate value, and $f_s$ [Hz] is sampling frequency. In the system, the carrier frequency, the chip rate, and sampling frequency are 24 kHz, 12 kcps (kilo chip per second) and 96 kHz, separately.

Sound signals from Speaker 1 and trigger signal from the Zigbee were synchronized emitted. After detecting the trigger signal in the receiver unit, the 0.25 second sound signal will be recorded, and the cross-correlation value is calculated by Eq.(2).

$$c(t) = \sum_{n=0}^{N-1} s(n)r(n+t) \quad (2)$$

where $n$ = 0, 1, 2 … $N$ - 1 ($N$ is the sample length). $t$ is the arrival time of the signal, $s(n)$ is the reference signal, $r(n)$ is the received signal. According to the calculated cross-correlation value, a normalized threshold calculated by Eq.(3), $C_{th}$, was used to distinguish a direct signal with reflected signals (Spachos et al., 2018).

$$C_{th} = C_{ave} + 4\sigma_{corr} \quad (3)$$

where $C_{ave}$ and $\sigma_{corr}$ are average absolute value and standard deviation of cross-correlation.

After getting the arrival time of SS Sound, the distance $d_j$ [m], from speaker to the microphone can be easily calculated by Eq.(4).

$$d_j = (331.5 + 0.61T\ ) \times \left(t_j - t_t\right) \tag{4}$$

where $T$ [˚C] is the temperature, $t_j$[s] is the arrival time of SS Sound obtained by cross-correlation and $t_t$ [s] is the received time in second of the trigger signal.

By using trilateration algorithm using at least three valid distances (Huang et al., 2020), the position of microphone could be estimated. In this experiment, four distances were used to calculate position.

## 2.2 Devices of SSSLPS

For the devices, the signals of spread spectrum sound were generated by a laptop computer (PC), converted from digital signal to analog signal at the audio interface (Fig.2.2) (Roland OCTA-CAPTURE UA-1010), amplified by amplifiers (Fig.2.3) (Kama Bay Amp Rev. B, Scythe Inc) and emitted by four twitters which are the high frequency response (Fig.2.4) speakers with 3D printed cone (Fig.2.5) (FT28D, Fostex Company). The sound level was set at 80dB using a noise meter (Fig.2.6) (LA-4440, Ono Sokki). Then, the emitted sound signal was received by a microphone at the same time, converted from analog signal to digital signal at the audio interface, and calculated at the PC. The reference is using the PC processed correlation calculation of sound signal, correlation peak detection to obtain received time of spread spectrum sound, and position estimation.


**Fig.2.2** Audio interface

**Table 2.1** Specifications of audio interface

| | |
|---|---|
| Number of channels | Sampling frequency＝44.1kHz、48kHz、96kHz<br>Recording ＝ 12 channel<br>Playback ＝ 10 channel<br>Sampling frequency＝192kHz<br>Recording ＝ 4 channel<br>Playback = 4 channel |
| Signal processing | PC interface＝24bit<br>AD/DA converter＝ 24 bit<br>Internal processing＝ 40 bit |
| Sampling frequency | AD/DA converter ＝ 44.1kHz, 48kHz, 96kHz, 192kHz<br>DIGITAL（IN/OUT）＝44.1kHz, 48kHz,96kHz |
| Specified input level (variable) | INPUT 1～6（XLR type）＝-56～-6dBu<br>INPUT 7～8（XLR type）＝-50～+0dBu<br>INPUT 1～8（TRS standard type）＝-46～+4dBu |
| Specified output level | OUTPUT 1～8＝+0dBu（バランス） |
| Frequency characteristic | 192.0kHz ＝ 60kHz～90kHz （+0/-8dB）<br>192.0kHz ＝ 20Hz～60kHz （+0/-2dB）<br>96.0kHz ＝ 20Hz～40kHz （+0/-2dB） |

| | |
|---|---|
| | 48.0kHz ＝ 20Hz～22kHz （+0/-2dB） |
| Noise level | INPUT 1～2→OUTPUT 1～2 ＝ -87dBu typ.<br>（GAIN：min.、Input 600 Ω termination、IHF-A）<br>※ InternalDirect Monitor Mixer Configuration：<br>Stereo Link＝on Input channel・Fader ＝ Unity |
| Dynamic range | AD INPUT 1～8＝104dB typ.（GAIN：min.）<br>DA （OUTPUT 1～8＝113dB typ.） |
| Interface | USB2.0（Hi-Speed）<br>Digital input / output（Coaxial・type）<br>MIDI Input / output |
| Power | DC9V（AC adapter） |
| Current | 1.45A |


**Fig.2.3** Amplifier

**Table 2.2** Specifications of noise meter

| | |
|---|---|
| Applicable standard | IEC 61672-1: 2002 Class 1 |
| Microphone | 1/2-inch backelectret-type<br>condensor microphone MI-1234<br>Nominal sensitivity level:－29 dB |
| Preamplifier | MI-3111 Preamplifier for mocrophone |
| Linearity range | 100 dB |
| Measurable frequency range | 10 Hz to 20 kHz (IEC, JIS) |
| Measurement level range | 35 to 137 dB (IEC, JIS) |
| Intrinsic noise | 27dB or less |
| Time weighting | FAST, SLOW, Impulse, 10 ms |
| Sampling interval | 20.8 μs (other than LN)<br>100 ms(LN) |
| Start mode | Manual, timer (time setting, in increment of 1 minute), trigger (can be started after a lapse of specified time [0 to 10 seconds, in increment of 1 second] after trigger detection: trigger delay function) |
| Display | LCD with LED backlight semitransparent (124 x 64-dot)<br>Measurement value display by numeric and bar indicators<br>List display and trend graph display for various kinds of calculated values<br>Displays of date, time, measurement time, and conditions of various kinds of instruments |

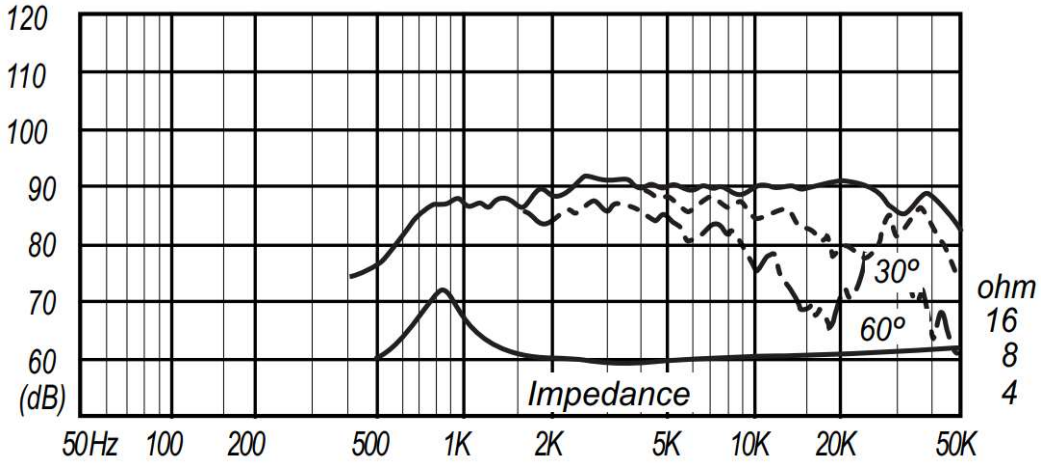


**Fig.2.4** Frequency response curve of speaker

**Fig.2.5** Speaker with 3D printed cone


**Fig.2.6** Noise meter

In this dissertation, a wireless system is used for positioning the moving robot in Chapter 5. The Zigbee (Fig.2.7) (3sZ11, System Watt) is used to emit and receive the trigger signal. The wireless receiving unit (Fig.2.8) consists of FPGA (EP4CE22F17C6N Cyclone IV, Altera) to record data and Jetson (Jetson Nano Developer Kit, Nvidia) for controlling robot and save data into a USB flash drive. The sound signal from two microphones with maximum 196 kHz sampling frequency, trigger signal from Zigbee, inertial measurement unit (IMU, MPU9250, InvenSense), magnetometer (HMC5883L, Honeywell), pressure sensor (MS5611-01BA, TE Connectivity) for estimating altitude, and thermometer (ADT7410, Analog Devices) data are recorded by the FPGA.

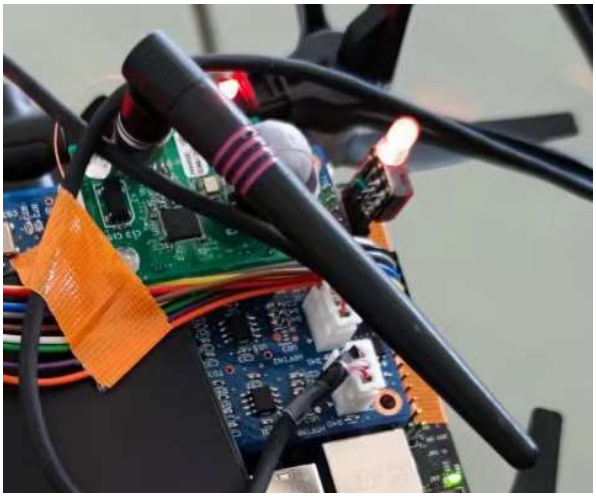

**Fig.2.7** Zigbee for transmitting and receiving the trigger signal

**Fig.2.8** Wireless receiving unit

# Chapter 3 Temperature Compensation System using Estimated Sound Velocity in a Small-scaled Greenhouse

## 3.1 Background

Spread Spectrum Sound-Based Local Positioning System (SSSLPS) has been developed for indoor agricultural robots. Such a SSSLPS has several advantages, including effective propagation, low cost, and ease of use. When using sound velocity for field position measurements in a greenhouse, spatial and temporal variations in temperature during the day can have a major effect on sound velocity and subsequent positioning accuracy. In this research, a temperature compensated sound velocity positioning was proposed and evaluated in comparison to a conventional temperature sensor method.

The SSSLPS determines position and provides localization inside a greenhouse based on the velocity of sound (Osada et al., 2003). However, the speed of sound propagation is affected by the spatial variation of temperature within a greenhouse (Wenzhou, 2019). We hypothesize that position and a more representative mean sound velocity within the greenhouse can be simultaneously determined using a time of arrival (ToA) localization algorithm (Ni et al., 2019; Widodo et al., 2013).

In this research, the objective is to develop a new temperature compensation method using an estimated sound velocity algorithm embedded in the spread spectrum sound-based local positioning system. To do this, we first developed a spread spectrum sound system that can generate the SS Sound signals. After that, the proposed temperature compensation method using a sound velocity estimation algorithm was compared with the conventional method of using temperature sensors. To evaluate field

*Full version of this chapter has been published in:*

*Tsay, L. W. J., Shiigi, T., Huang, Z., Zhao, X., Suzuki, T., Ogawa, Y.,Kondo, N.(**2020**). Temperature-Compensated Spread Spectrum Sound-Based Local Positioning System for Greenhouse Operations. IoT. 1. 147-160*

performance of the proposed estimation method, experiments were conducted in a small-sized greenhouse in summer and winter, when temperature variations are expected to be extreme. We also analyzed the positioning accuracy of the temperature compensation methods as well as the extent of temperature fluctuations within the greenhouse at these times.

Moreover, the accuracy of this indoor spread spectrum sound localization system can be improved by directly calculating position and estimating sound velocity simultaneously based on a ToA algorithm (Le and Ono, 2014). Moreover, ToA localization does not require as many nodes to detect position as other localization algorithms.

## 3.2 Proposed Algorithm

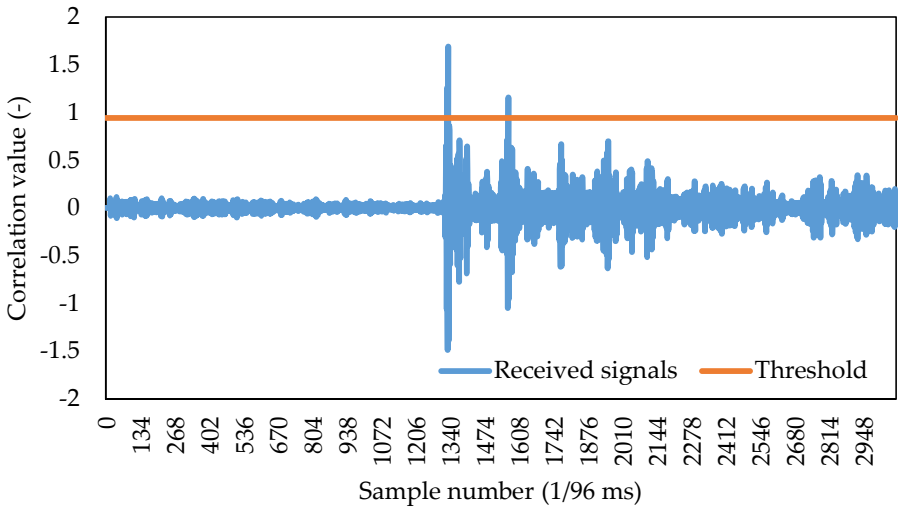


**Fig.3.1** Normalized correlation value and threshold for peak detection from received signals

The sound velocity parameter in Eq.(5) is sensitive to temperature; thus, the conventional means to compensate for this is using a precise temperature measurement (sensor) taken at speaker $i$ to get the $T_{si}$ to calculate the distance $d_i$ from the speaker $i$ to the microphone target by the following Eq.(6):

$$v_i = 331.5 + 0.61(T_{si}) \tag{5}$$

$$d_i = (v_i)(t_i) \tag{6}$$

where $T_{si}$ is the temperature at speaker $i$, $v_i$ is the speed of sound signals (m/s) and $t_i$ is the propagation time of emitted sound from the $i$th node in a GPS-like system, which refers to the target passively receiving the navigation signal (Matano and Tanaka, 2003). In Fig.3.1, the propagation time is the first detected peak of the sample number (1/96 ms). Multiplying the propagation time with the sound velocity will give a distance measurement result. At last, three known distances are needed to get a position using trilateration in the conventional method.

The proposed method using an estimated sound velocity for calculating the position and the sound velocity is based on a ToA localization algorithm. Eq.(5) indicates the relationship between distances and coordinates of each node and measurement position simultaneously. This differs from the conventional method (Eq.(4)), which uses data from temperature sensors (Le and Ono, 2015).

$$(t_i)(v_e) = \sqrt{(x_s - x_i)^2 + (y_s - y_i)^2 + (z_s - z_i)^2} \tag{7}$$

$$f_i(x_s, y_s, z_s, v_e) = \sqrt{(x_{s0} - x_i)^2 + (y_{s0} - y_i)^2 + (z_{s0} - z_i)^2} - (t_i)(v_e)$$

where, $t_i$ is propagation time of emitted sound of the $i$th node, $(x_s, y_s, z_s)$ is the estimated position of the target, $(x_i, y_i, z_i)$ is the position of the $i$th node, $(v_e)$ is the estimated sound velocity. It is assumed in Eq.(7) that the sound velocity of the propagated sound between the transmitters and receiver in the greenhouse is constant.

The unknowns are the position coordinates $(x_s, y_s, z_s)$ and the estimated sound velocity $(v_e)$. When the transmitting time $(t_i)$ is measured, the positions of the nodes

are known and the provisional sound velocity can be set. Therefore, the four unknowns $(x_s, y_s, z_s)$ and $(v_e)$ can be estimated when the number of nodes is larger than four, since at least a system of four equations in Eq.(7) are needed in order to solve the four unknowns. The function, $f_i(x_s, y_s, z_s, v_e)$, represents the positioning error, which indicates the distance of the target position minus the sound propagation distance.

This is difficult to compute because Eq.(7) is a non-linear equation.. Thus, it needs to be linearized by a Taylor expansion, $(x_s, y_s, z_s)$ and $(v_e)$ estimated by sequential computation of the function $f_i(x_s, y_s, z_s, v_e)$, which is also defined in Eq.(5). $f_i(x_s, y_s, z_s, v_e)$ is linearized by the first-order Taylor-series expansion at $x_{s0}, y_{s0}, z_{s0}, v_{e0}$, as in Eq.(8).

$$\begin{aligned} f_i(x_s, y_s, z_s, v_e) = {} & \sqrt{(x_{s0} - x_i)^2 + (y_{s0} - y_i)^2 + (z_{s0} - z_i)^2} - (t_i)v_{e0} \\ & + \frac{\partial f_i}{\partial x_s}(x_s - x_{s0}) + \frac{\partial f_i}{\partial y_s}(y_s - y_{s0}) \\ & + \frac{\partial f_i}{\partial z_s}(z_s - z_{s0}) + \frac{\partial f_i}{\partial v_e}(v_e - v_{e0}) \end{aligned} \tag{8}$$

The defined matrixes and vectors are as in Eq.(9)

$$\Delta d_i = \frac{\partial f_i}{\partial x_s}\Delta x_s + \frac{\partial f_i}{\partial y_s}\Delta y_s + \frac{\partial f_i}{\partial z_s}\Delta z_s + \frac{\partial f_i}{\partial v_e}\Delta v_e$$

$$\Delta x_s = (x_s - x_{s0})$$

$$\Delta y_s = (y_s - y_{s0})$$

$$\Delta z_s = (z_s - z_{s0})$$

$$\Delta v_e = (v_e - v_{e0})$$

$$\Delta d = \begin{bmatrix} \Delta d_2 \\ \Delta d_3 \\ \vdots \end{bmatrix} \qquad A = \begin{bmatrix} \frac{\partial f_2}{\partial x_s} & \frac{\partial f_2}{\partial y_s} & \frac{\partial f_2}{\partial z_s} & \frac{\partial f_2}{\partial v_e} \\ \frac{\partial f_3}{\partial x_s} & \frac{\partial f_3}{\partial y_s} & \frac{\partial f_3}{\partial z_s} & \frac{\partial f_3}{\partial v_e} \\ \vdots & \vdots & \vdots & \vdots \end{bmatrix} \tag{9}$$

$$\Delta x = [\Delta x_s \quad \Delta y_s \quad \Delta z_s \quad \Delta v_e]^T$$

$$\Delta d = A \Delta x$$

$A$ is the observation matrix. The generalized inverse matrix of $A$ is multiplied on both sides of the Eq.(10). An iterative least squares method is used by iterating 50 times when $\Delta x$ is approaching 0 and gives the approximate coordinate of the target.

$$\Delta x = (A^T A)^{-1} A^T \Delta d \tag{10}$$

## 3.3 Materials and Methods

A ridged greenhouse without plants to interfere with the path of the sound signal was used as the target localization area. With doors shut, no ventilation open, or wind inside for the experiment. For this small-sized greenhouse, a set of four speakers and a microphone are adequate. Temperature variations within the greenhouse can have a major effect on the sound-based system since the greenhouse covering was made from common polyethylene plastic, which enables radiation heating.

The SS Sound signals were generated by a laptop computer (PC), converted from digital to analog signals at the audio interface (Roland OCTA-CAPTURE UA-1010), amplified by amplifiers (Kama Bay Amp Rev. B, Scythe Inc) and emitted by four twitters, which are high frequency speakers (FT28D, Fostex Company). Before the experiment, the sound level was calibrated at 80 dB using a noise meter (LA-4440, Ono Sokki). Then, emitted sound was received by a microphone (M30, Earthworks), converted from analog to digital signals at the audio interface, and the position coordinates calculated at the PC. The computer processed the correlation calculation of the received sound signals, getting a correlation peak to obtain received time of spread spectrum sound, and position estimation. The M-sequence's period was 1023, with is also

combined with the time division multiple access (TDMA) method. Fig.3.2 shows outline of the localization system.

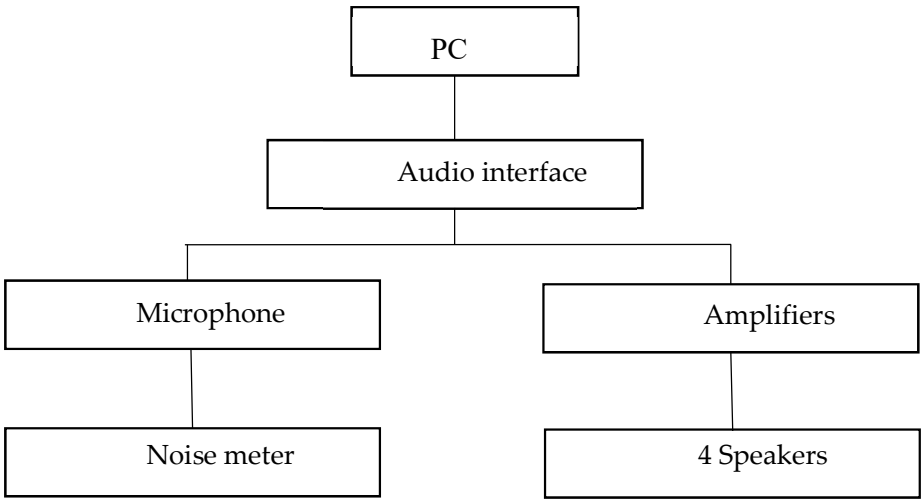


**Fig.3.2** Devices connection of the localization system

The experiment was conducted in a typical farmer's small greenhouse (Fig.3.3) (width 3.5 m x length 13 m x height 2 m) in Toon-shi of Ehime prefecture, Japan. The experimental greenhouse was recovered with new polyethylene film before the experiment in order to fit the condition for controlling for air ventilation. Fig.3.3 shows the front door, as well as the orientation of the greenhouse after the recovering and Fig3.4(a) shows the four speakers, the total station at the edges for reference coordinates and the overall setup of the experiment, which was conducted on a sunny summer day with local temperature ranging from 20 to 34 °C (27$^{th}$ September 2018). There was some drizzle in the morning. Fig3.4(b) shows the experiment conditions where some radish plants were growing in the greenhouse on a cloudy winter day where temperatures ranged from 0 to 10 °C (23$^{rd}$ January 2019).


**Fig.3.3** Front of the greenhouse and the north direction

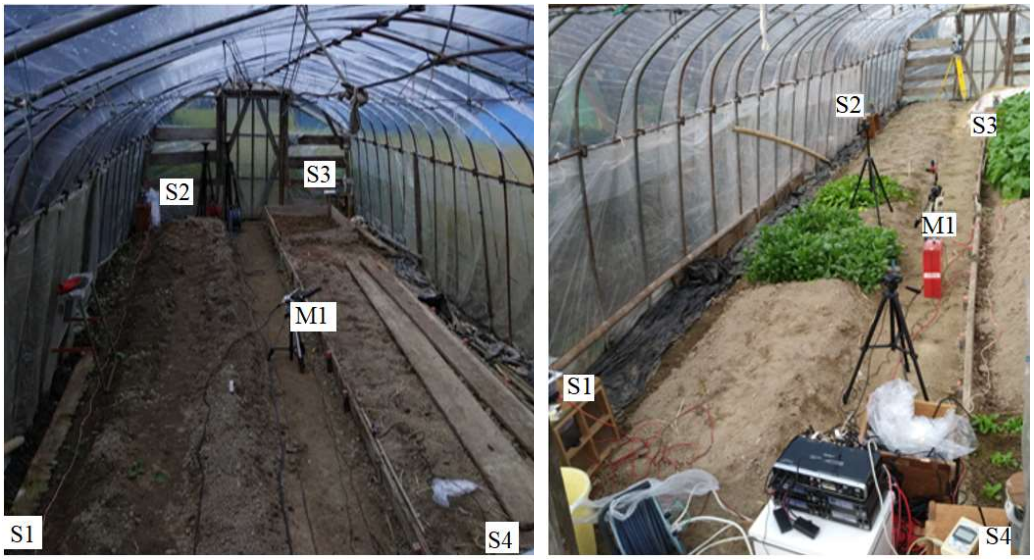


**(a)** **(b)**

**Fig.3.4 (a)** Speakers and microphone setting in the greenhouse in summer; **(b)** Similar settings in winter whilst there were some radish plants in the field

Fig.3.5 illustrates the experimental localization area, as well as the settings of the speakers and microphone. The whole experiment was conducted in a closed greenhouse

with the greenhouse doors shut most of the time during the two days of the experiment. There were no people inside the greenhouse during the measurements. The experiment started from 10:00 to 19:00 with temperatures recorded hourly (a total of 10 measurements) and SS Sound data recorded at least 6 times at each sampling. Recorded temperatures ranged from 4 to 38 ℃, the typical range found in greenhouse farming situations. The outside temperature ranged from 0 to 27 ℃. It is believed that the temperature data obtained covers typical greenhouse temperatures in winter, as well as in summer and is representative of the potential influences of temperature variation on the spread spectrum sound localization system.

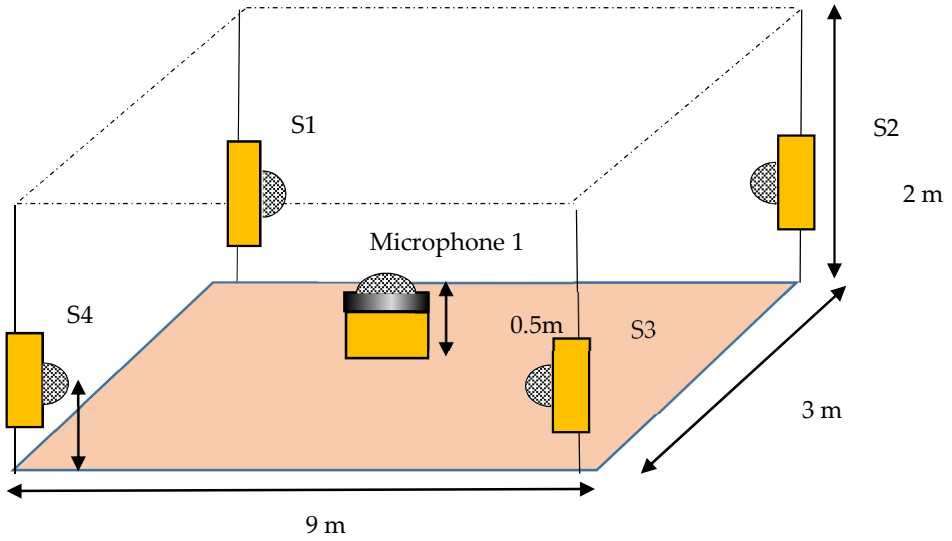


**Fig.3.5** Speakers and microphone position and the size of measurement field

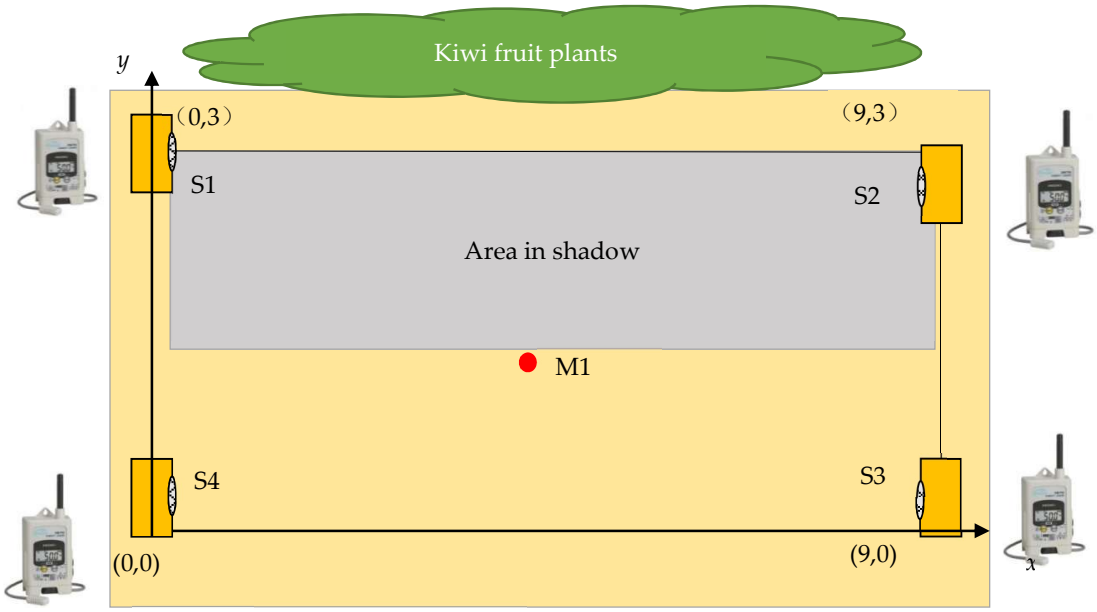


**Fig.3.6** Measurement area, position of nodes and the four temperature sensors in 2-dimensional plane

Fig.3.6 shows the setup of the four speakers with their accompanying temperature sensors that the total station measured the distances, from Speaker 1 (S1) to Speaker 4 (S4) was 3 m and the distance from Speaker 1 (S1) to Speaker 2 (S2) was 9 m. There were some kiwi fruit plants outside the greenhouse creating some shades covering the area where Speaker 1 and Speaker 2 were. The recorded temperatures are expected to be lower than those at Speaker 3 and Speaker 4.

Fig.3.7 shows the horizontal view of the experimental setting, showing the speaker and measurement positions (50 cm above the ground) were higher than the ridges. Since all the nodes were set at a 50 cm height above ground, the calculated target position was determined in 2-dimensional coordinates. Fig.3.8 illustrates the actual experiment conditions with temperature sensor covered by a wind tube (Fig.3.8(a)) and microphone fixed at 50 cm height (Fig.3.8(b)). A fan inside the wind tube was switched on to increase equilibration with the surrounding air temperature. The tube was placed a few centimeters below the speakers.

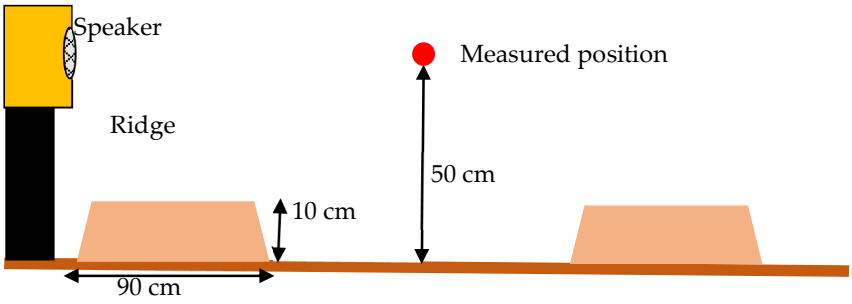


**Fig.3.7** Horizontal view of the speaker and microphone

**(a)** **(b)**

**Fig.3.8** (**a**) Temperature sensor with wind tube placed near speaker at 50 cm; (**b**) Microphone at the center of the greenhouse, 50 cm aboveground.

## 3.4 Results and discussion

### 3.4.1 Evaluation of the temperature in greenhouse

Temperature differed at each speaker within the greenhouse (0.5 m above ground). Moreover, the speakers (S1 and S2) in shaded areas had lower temperatures due to the

received radiation energy being reduced. Fig.3.9 shows the results of greenhouse temperature data at the four speakers during a typical summer season (the upper four curves) and winter season (the lower four curves) which represents a temperature range from 2 ℃ in winter up to 35 ℃ in summer. It was observed that maximum temperature differential can be up to 11 ℃ when the sun rays at their strongest (14:00 in winter). However, after sunset in summer (17:00) and in winter (16:00), temperatures dropped making any temperature differences in the greenhouse negligible.

Microclimate phenomenon, small areas with differing atmospheric conditions (Li et al., 2018) occurred during the day and created approximately 6 ℃ differences within the greenhouse. A convective heat transfer was observed as the warm moist air rose to the top and condensed on the walls of the greenhouse. Such condensation would not happen if there was air flow or ventilation in the greenhouse (Kumar, 2017). The temperature distribution during the daytime was more uniform in the summer than the winter (Perret et al., 2005) and created horizontal regions of temperature differences in the greenhouse. During the summer, experiment recordings were paused temporarily at 12:15 to open the greenhouse door for 30 minutes to reduce overheating in the greenhouse. Thus, there was a temperature drop at 13:00 in the summer of approximately 5 ℃.

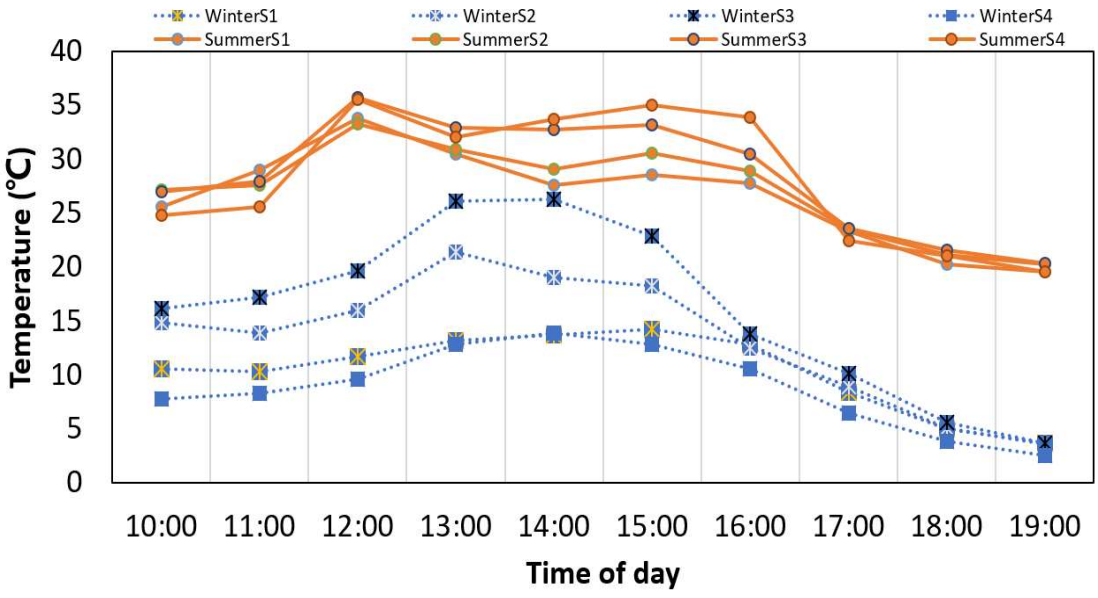


**Fig.3.9** Temperatures of speakers in greenhouse

### 3.4.2 Comparison of conventional temperature sensor method and estimated sound velocity method

Fig.3.10 shows the average position error of the conventional temperature sensor method (sensor method) and estimated sound velocity method (estimated method) in summer. The sensor method uses temperature sensor data to calculate the sound velocity and then calculates the position results, whilst the estimated method uses the estimated sound velocity to calculate the position results directly. The average position error for the sensor method was 23.12 mm, while for the estimated method had only a 11.14 mm error. In Fig.3.9, the largest temperature differences occurred at 15:00. This is consistent with the sensor method generating a large positioning error when the temperature differences within the greenhouse were large. The sensor method was more accurate at 17:00 when the temperature difference between the speakers was minimal. At this time, both methods had a position error around 20 mm. The estimated method was not as accurate at 12:00, as well as at 16:00, as other times between dawn and dusk. These two periods correspond to times when there were rapid changes in temperature within the greenhouse. Consistent with temperature variations (at different speakers) adversely affecting sound velocity estimates within the greenhouse. Temperature sensors merely measure and record the temperature near the sensor (speaker), thus they do not accurately reflect the temperature over the whole sound propagation pathway.

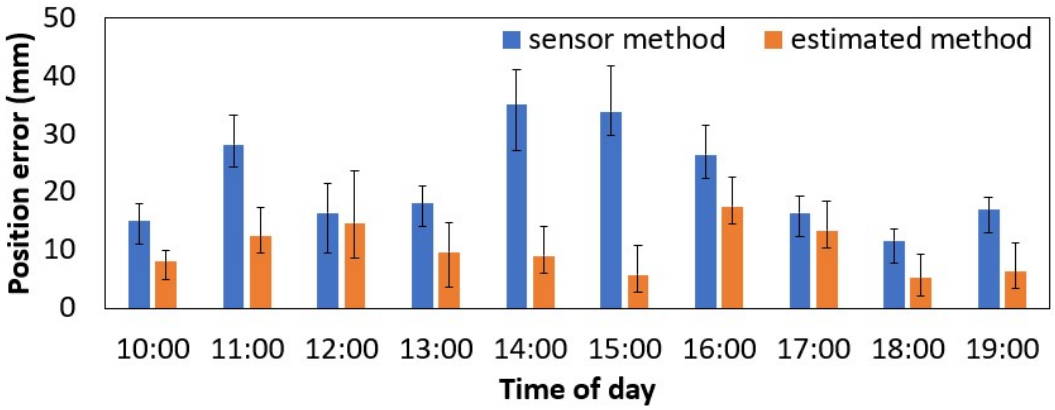


**Fig.3.10** Position error of the sensor and estimated methods in summer

Similarly, Fig.3.11 shows the average position error in winter was 38.94 mm using the sensor method, while the average error was 17.17 mm using the estimated method. Compared to the summer results, the winter temperature differences in the greenhouse

propagated larger positioning errors for the sensor method than for the estimated method throughout the whole day. In winter when the outside is lower than that inside the greenhouse, larger temperature variations within the greenhouse can be generated with fluctuating sunlight radiation levels. Moreover, water vapor lost (transpiration) from the leaves of the radish plants' may also have affected sound velocities in the winter experiment; giving rise to larger position errors in winter compared to summer for both temperature compensation methods.

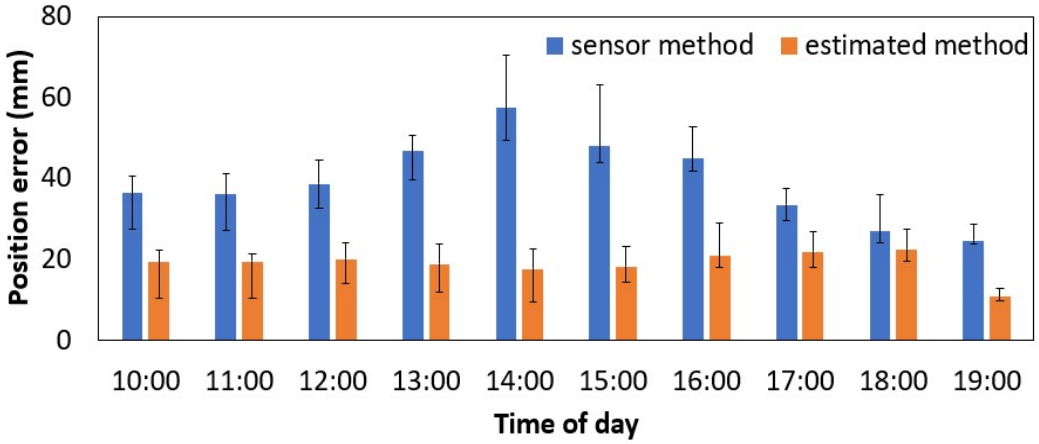


**Fig.3.11** Position error of the sensor and estimated methods in winter

Fig.3.12 shows the relationship between position error and temperature differences in the greenhouse for both the summer and winter experiments. Position errors can be generated by errors in sound velocity estimates due to temperature variations along the signal transmission path. The standard deviation of temperature used in Fig.3.12 was calculated from the four temperature sensors placed at each of the speakers during the experiment. Temperature differences in the greenhouse in winter, as measured by the sensor method, were larger than those observed in the summer experiment, as were the observed positioning errors. As the desired precision was set to a minimum of 20 mm in a previous study (Widodo et al., 2013), the estimated method achieved results that were more stable and closer to the desired precision than those achieved by the sensor method.

Though the estimated sound velocity method assumes that sound velocity is uniformly distributed, the result shows that it can tolerate uneven sound velocity

generated by large temperature differences within a small-sized greenhouse. The results demonstrate that the estimated method better reflects actual sound velocities within the greenhouse, and thus provides more accurate positioning results than the sensor method (position errors at or below the 20 mm limit). The proposed algorithm approximates the average sound velocity along the whole signal transmission path better than the conventional calculation does.

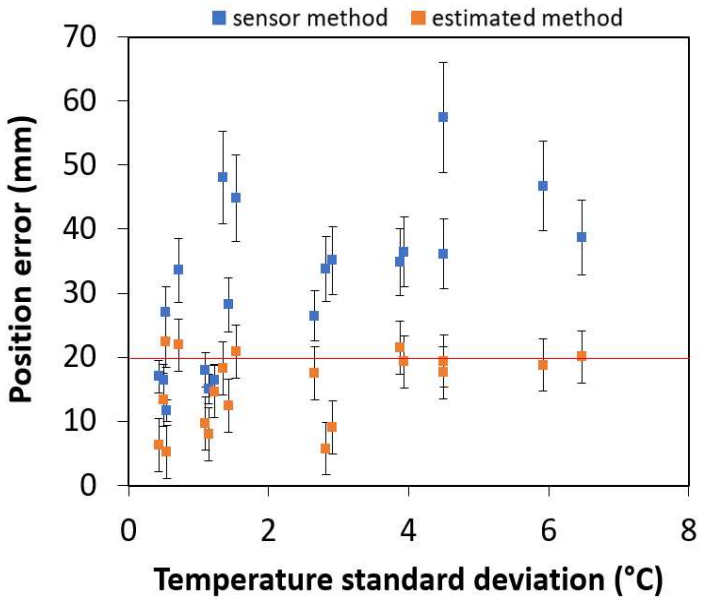


**Fig.3.12** Relationship between position error of the two methods and temperature standard deviation

In this research a proposed estimated method for estimating average temperature along the propagated sound path is used to estimate average sound velocity between the transmitter and receivers. When temperatures varied substantially within the greenhouse, this average temperature estimation method was more accurate at deriving sound velocity than the conventional sensor method, which uses local temperature sensor measurements at each node.

To evaluate the accuracy of this new temperature compensation method embedded in an SSSLPS system, positioning measurements were undertaken both in summer and winter when seasonal variations in temperature within the greenhouse are expected to be at their largest. Temperature variations of up to 11 °C were observed in winter, while

variations less than 6 °C were observed in summer, resulting in differences in positioning accuracy of around 5 – 10 mm between the two seasons. The low outside temperature in winter created large fluctuations in the daytime temperature within the greenhouse, whilst we speculated that the transpiration from the radish plants' growing there at the time also affected surrounding air temperature and humidity variation within the greenhouse (Yang et al., 1990). Microclimatic temperature layers inside the greenhouse (Li et al., 2018), especially in winter, effectively trap hot air and generate convection phenomenon with the surrounding cold air.

To evaluate and compare the positioning accuracy of the estimated versus the conventional sensor method, average positioning performance was measured, with the estimated method achieving a better position accuracy than the desired precision of less than 20 mm. The overall positioning accuracy of the estimated method (14 mm) was higher than the sensor method (30 mm) for the combined summer and winter results. The estimated method has the advantage of simultaneously calculating position and estimating sound velocity compared to the sensor method, but the calculation is more complicated and requires more nodes. Positioning errors can also be affected by the signal time of arrival measurement errors, as well as the setting error associated with total station measurement errors, etc.

## 3.5 Conclusions

This research proposed a new temperature compensation method that can be used with localization systems that estimate position using sound for accurate positioning inside small-sized greenhouses. Results indicate this new proposed method has a positioning accuracy to within 20 mm in a 3 m x 9 m ridged greenhouse. It has the potential to replace the current system of using the temperature sensors in a greenhouse.

The summer and winter experimental result demonstrate that the newly developed

temperature compensation method does not require the setup of temperature sensors, while providing similar or even better positioning accuracy than compensation based on conventional temperature sensor measurements. The estimate algorithm works well in a small controlled indoor environment and can predict the average sound velocity along the propagated path between the transmitters and receiver. This also means that the proposed estimated method can compensate for temperature-generated errors in an SSSLPS used in the small-sized greenhouse.

This new temperature compensation method achieved a positioning error using SSSLPS at or below 20 mm during the season, even at extremes in summer and winter. This accuracy can outperform most of the existing positioning systems and can be used to control multiple robots, such as ground vehicles, in a greenhouse. By simultaneously calculating the position and estimating the average sound velocity, more convenient temperature compensation in a greenhouse is achieved without the need to use temperature sensors. It should be noted that both calculations are based on a ToA algorithm. It is believed that the SSSLPS can contribute greatly to the development of IoT in agriculture and indoor precision agriculture.

# Chapter 4 Static and Dynamic Evaluation of Acoustic Positioning System Based on TDMA & FDMA for Robots Operating in a Greenhouse

## 4.1 Background

The SSSLPS have high tolerance to noise, but due to the signal of a further source weaken, which make the receiver hard to detect it as the signal from a nearer source stay strong. This signal co-channel interference problem also referred to as “signal crosstalk”. The effective range of SS Sound positioning system is heavily limited. The receiver is hard to detect the weakened signals if the signal is far away from the source because when the signals from a nearer source stays strong, there is a channel interference between the speakers which is also referred to the ‘near-far problem’ (Madhani et al., 2003).

Conventional research used different codes to classify acoustic signals using code-division multiple access (CDMA) method (Aguilera et al., 2015), but it was not suitable for a greenhouse application due to the system settings. For example, in Fig.4.1, when the Receiver wants to receive a clear signal from Emitter 1, the signal from Emitter 2 becomes the noise source. In a greenhouse application, distance between Emitter 2 and Receiver can be 1 m, and the distance between Emitter 1 to the Receiver can be much larger. For tackling near-far problem, multiple access methods in signal processing communication were studied and there are two main methods, the frequency division multiple access (FDMA) and time division multiple access (TDMA), are suitable for SS Sound signals as the former one uses the frequency bandwidth to separate the channel interference and the latter one separates the sound in time domain. FDMA has the advantages of getting a fast synchronized measurement since many signals can be transmitted in different frequencies at the same time while the advantages of TDMA are having a longer signal for a better noise tolerance and easier to detect the correct

peak. However, the disadvantages of FDMA are the sound level damping in high frequency area and also it is difficult to detect the correct peak (Huang et al., 2020). TDMA has a limitation in time delay which is an obvious drawback, as the signals take time to be transmitted and they need to wait before the next sound wave is being emitted. However, the time delay issue is not a problem when measuring static location but it might create a problem if TDMA needs to detect a moving target.

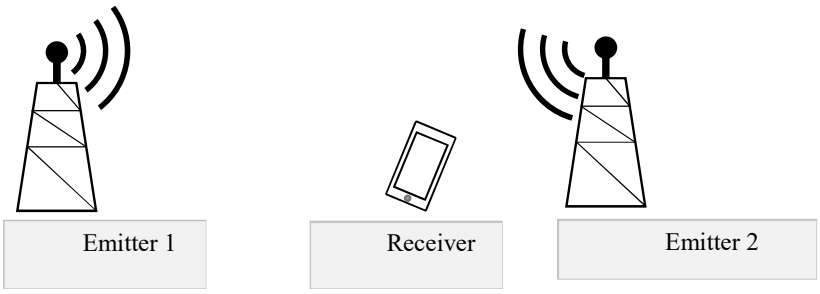


**Fig.4.1.** Near-far problem

In this research, we investigated two channel access methods, FDMA and TDMA to be applied to the SSSLPS system for positioning a target in a greenhouse and solving the near-far problem. We did experiment in an actual commercialized greenhouse for static measurement and then we also conducted the dynamic measurement using the motion capture system in a laboratory. The signal properties, system performances as well as the effectiveness against the near-far problem with those two methods would be evaluated and discussed.

## 4.2 Material and Methods

### 4.2.1 TDMA & FDMA methods

Using TDMA method, the speakers will insert a time interval to avoid transmitting in the same time slot. To make sure that signals arrive at different time slots, the time interval should be adjusted according to the operation area. The frequency of transmitting signal which means the measurement in one second, is set at 4 Hz. The

scheme of emitting the TDMA sound signal is showed in Fig.4.2.

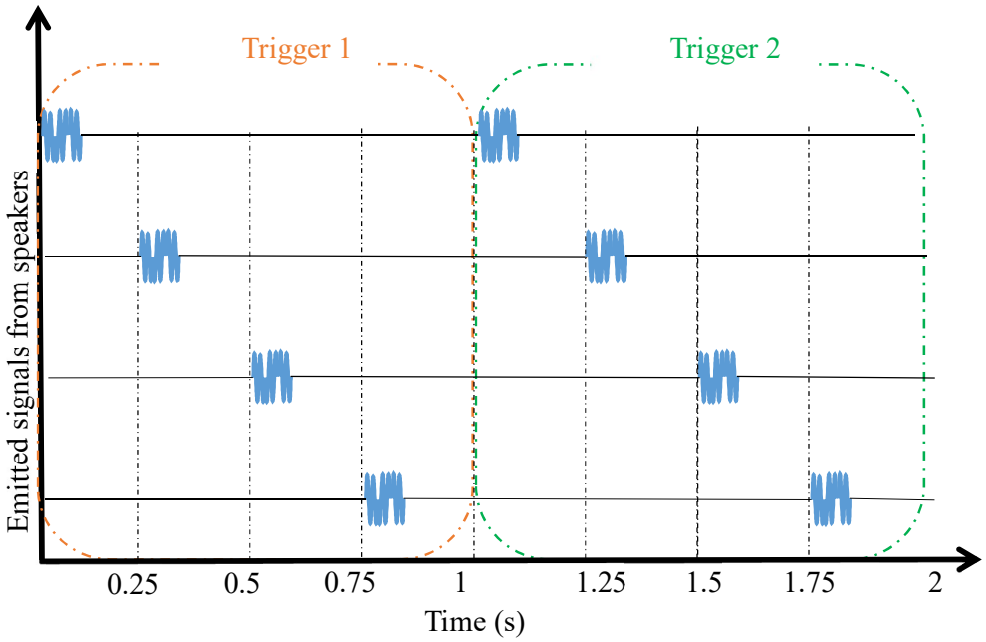


**Fig.4.2** Emitted TDMA signals of four speakers

Although the signals properties were set the same, but every signal is emitted in different time. The time length of each TDMA signal package is 1 second. Thus, the time interval between every effective signal would be 0.25 s. Each time interval passed, a new range will be update. The position will use the updated distance and previous three updated ranges from different speakers to calculate the coordinates of the robot. For example, at 1.25 s in Fig.4.3, besides the distance data provided of S1 from trigger 2, the distance data from S2, S3, S4 from trigger 1 are used for the position calculation.

When the target is in a dynamic state such that moving towards a direction, TDMA will encounter a time delay problem for the moving distance since there is a delay time from the separated time slots and results in an area of the possible target position.

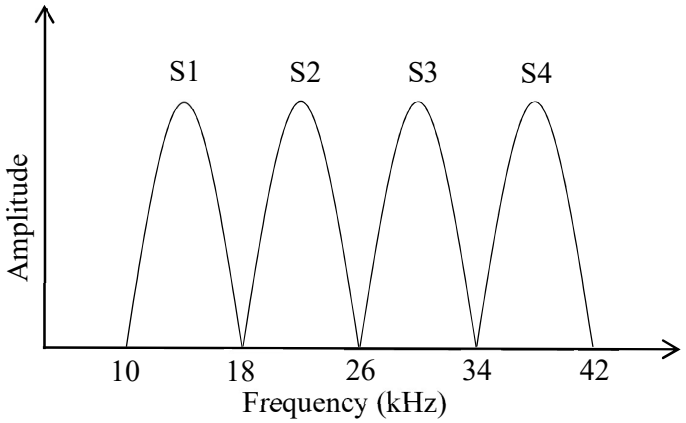


**Fig.4.3** The FDMA signal frequency spectrum

For FDMA method, the signals' frequency spectrum will be rearranged. As Fig.4.3 shows, the signal frequencies of speakers are arranged in separate regions of frequency spectrum. This method divides the bandwidth into four and allocate to different speakers. Conventionally, the bandwidth is divided into non-overlapping frequency sub-channels. To split the wide bandwidth of signal frequency of original signal, which will lose the advantage of broad signal properties, such as graceful degradation and less bandwidth expansion (Rajendra et al., 2009). With a small SS Sound signal bandwidth, peak detection problems will occur as the disadvantage. Therefore, we tried different signal overlap rates to show the channel interference at different signal bandwidths.

We prepared four different signals to conduct the experiment as Table 4.1 shows. The first two signals TDMA and FDMA were used for comparing the two methods with each other, including the signal strength SNR, ranging and positioning accuracy. The last three signals, FDMA-I, FDMA-II, FDMA-III, are aiming to compare the FDMA signals. The percentage in Table 4.1 means that the overlap rate of the frequency bandwidth of each signal to one of its adjacent signals. The minimum frequency of these signals is set to 10 kHz, which not only ensures that the system is not affected by the noise of agricultural machinery (Widodo, 2013), but also does not produce strong

noise to people. According to the Canadian federal noise regulations (Penney, 2016), there is only has permissible exposure time that over 85 dB. So, if the human works 0.5 m away to the speaker, there is no such exposure time limitation.

**Table 4.1** Properties of SS Sound signals

| **Signals** | $f_c$ **(kHz)** | $f_{chip}$ **(kcps)** | **M-sequence length** |
|---|---|---|---|
| TDMA | 24 | 12 | 1023 |
| FDMA-I (0%) | 14, 22, 30, 38 | 4 | 511 |
| FDMA-II (25%) | 14, 20, 26, 32 | 4 | 511 |
| FDMA-III (50%) | 14, 18, 22, 26 | 4 | 511 |

### 4.2.2 Static experiment

The sound signal will be generated by PC and be processed by audio interface (OCTA-CAPTURE UA-1010, Roland). Audio interface will convert the digital signal to analog signal. The Amplifiers (Kama Bay Amp Rev. B, Scythe Inc.) will amplify the signal. Then, the SS Sound signal will be emitted by speakers (FT28D, Fostex Company), received by a microphone (SPM0404UD5, Knowles Electronics). To make sure the four speakers output power are the same, the measured sound signal was a uniformed Gaussian white noise. Then, the sound level is evaluated by a noise meter (LA-4440, Ono Sokki) at 90 dB (at a distance of 10 cm to the center of speaker) using white noise. The thermometers (3670, Hioki) were set near to the speakers and microphone to record temperature data. The ground true position data of speakers and microphone was acquired by a total station (SRX5XT 32T-11, Sokkia) with (1.5 + 2 ppm × measurement distance) mm accuracy.

The experimental area was set 8.3 m × 22 m rectangle area, which covered half of the total greenhouse area. The greenhouse from Fig.4.4(a) is table-cultured without any plants or obstacles in target area, tables are 1m above the ground. The doors and

windows were shut down to prevent ventilation. The speakers were set at 1.5 m above the ground at the four corners of the target area. One quarter of the experiment area Fig.4.4(b) was measured, and the middle corridor was also included. The total station is set next to the field so that it can generate the reference coordinate for all the devices.

The microphone stand, 1.3 m above ground, was placed at the points and then began the measurement. To focus on the near-far problem, the obstacle on the sound path were avoided since it may lead to a multi-path effect of sound signals. After the measurement (four signals by order (Table 4.1)) finished, the microphone stand was moved to the next point. The microphone was always set to face the direction of the side between Speaker 1 and Speaker 2 to ensure the worst situation of Speaker 4 and Speaker 3, which were most influenced by channel interference (near-far problem) in the experiment condition. At each measured position, the signals were measured one by one, and each signal was measured 20 times.

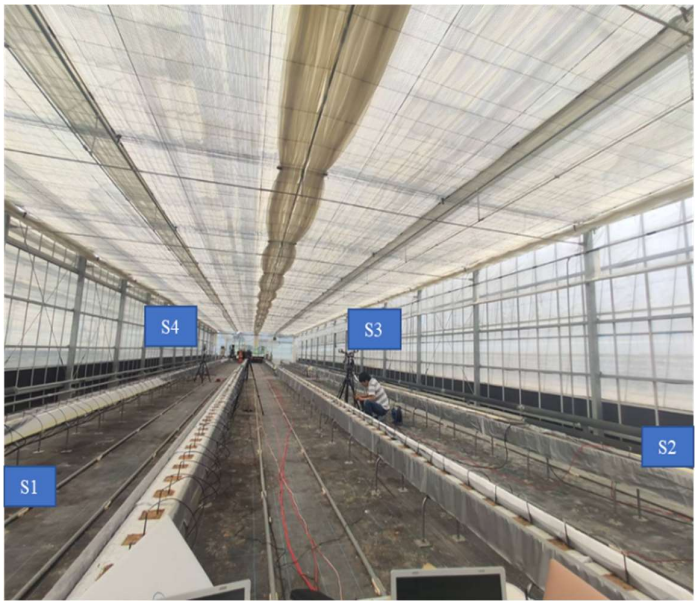


(a)

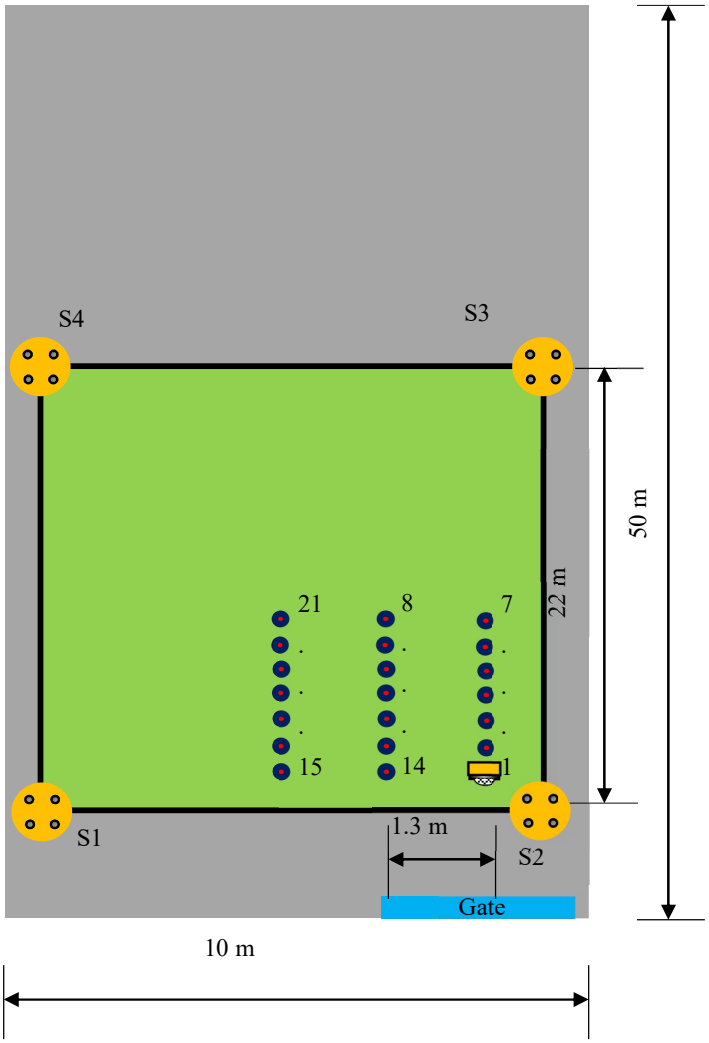


(b)

**Fig.4.4** Insides of (a) Kizu greenhouse and (b) the experiment setup

### 4.2.3 Dynamic experiment

Besides the device used in the greenhouse experiment, for the dynamic experiment we used the wireless trigger signal which was emitted by the Zigbee device, the four speakers are set at 2 ± 0.04 m height at four corners and we also added the Doppler compensation algorithm (Huang et al., 2021) in the distance calculation. Meanwhile, the motion capture system (Vicon Tracker, Vicon Industries Inc.), with 0.15 mm

accuracy (Merriaux et al., 2017), was used with 8 cameras at the edges for providing the reference position to evaluate the accuracy of SSSLPS during movement. For the dynamic settings, the experimental area reduced to 7 m × 5 m because of the limitation of the camera-based motion capture system that cameras were put at four corners and the middle of each edge, SSSLPS receiver got the emit time of SS Sound by measuring received time of trigger 1. The other trigger signal was emitted and received by audio interface. We then calibrated motion capture coordinates with SS Sound coordinates provided from total station.

By using 18 points of position data, we transformed the coordinates at S1 to be the origin (0,0), S1 to S2 as x-axis and S1 to S3 as y-axis. The SS Sound receiver was recognized as a motion capture model attaching 4 markers on it and was mounted on a crawler robot, which was controlled wirelessly and moved along the write arrow in Fig.4.5 at a low velocity around 300 mm/s and we repeated the experiment four times.

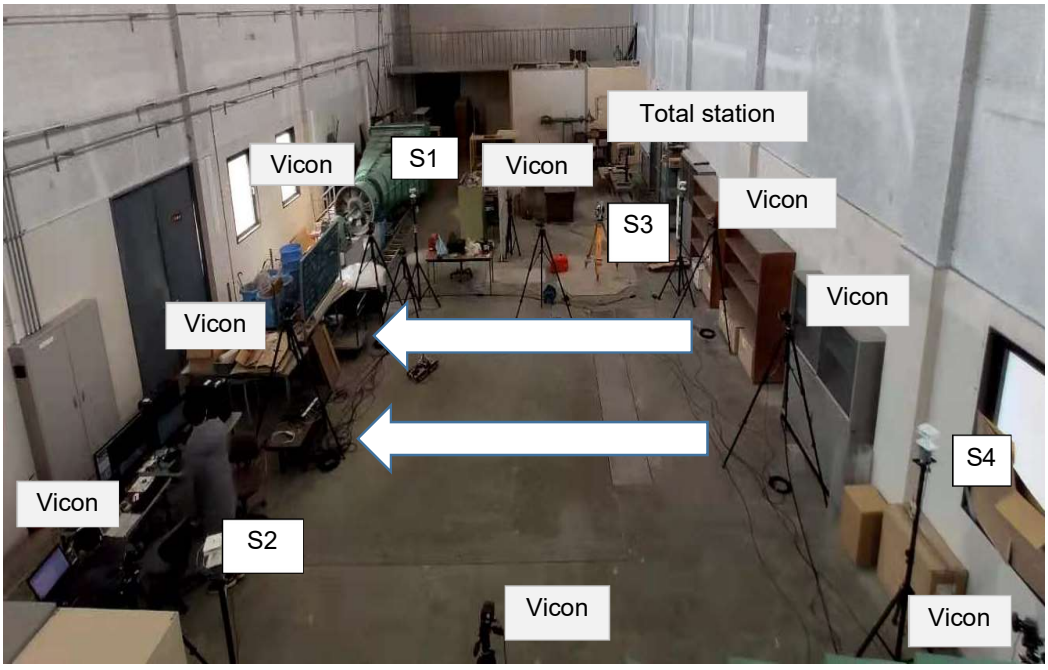


**Fig.4.5** Experiment setup of dynamic measurement

Since the final goal is to operate the SSSLPS in an actual greenhouse, the experimental greenhouse setting was used for TDMA simulation at different moving speed from 100 mm/s to 1000 mm/s. The robot was moving along the five tables with a range error of 25 mm and we repeated the simulation measurement for 10 times.

## 4.3 Results and discussion

### 4.3.1 Static positioning of TDMA and FDMA

In this research, we focus on 2D mean absolute positioning error so that the x, y coordinates differences would be evaluated. As introduced above, the error is calculated according to the reference ground truth measured by the total station. The detection rate was defined as the position error is less than 100 mm which is similar accuracy with Ultra-Wideband (Delamare et al., 2019). We calculated the detection rate for all the methods, the positioning error and also the range error from the four speakers. During the whole experiment period, indoor temperature was at a stable 24 ± 0.6 °C which means that the sound velocity in the greenhouse is remain evenly distributed.

**Table 4.2** Results of the 21 statics points in Kizu greenhouse

| **Signals** | **Detection rate** | **2D error (mm)** | **Range error (mm)** |
|---|---|---|---|
| TDMA | 100% | 12.2 ± 8.1 | 12.6 ± 7.7 |
| FDMA-I (0%) | 91% | 31.6 ± 17.5 | 19.9 ± 18.9 |
| FDMA-II (25%) | 71% | 52.0 ± 45.4 | 34.8 ± 52.3 |
| FDMA-III (50%) | 55% | 33.1 ± 37.7 | 25.9 ± 48.5 |

Table 4.2 shows TDMA has 100% detection rate and FDMA-I has 91% detection rate, while overlapped FDMA-II and FDMA-III only have 71% and 55% detection rate. It is clearly to see that TDMA has the best results while FDMA-III (50% overlapped

signals) has the worst detection rate. FDMA has a worse overall performance than TDMA.

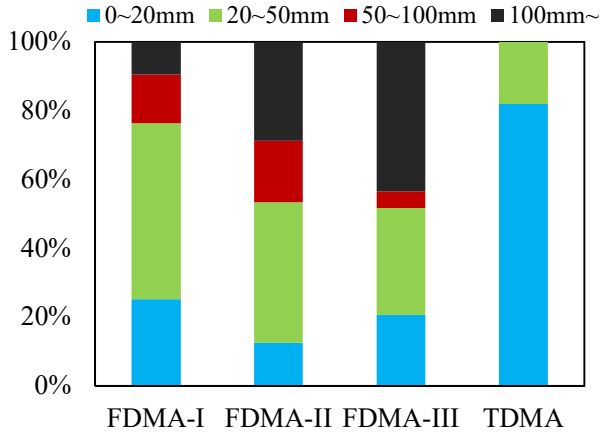


**Fig.4.6** 2D positioning error distribution

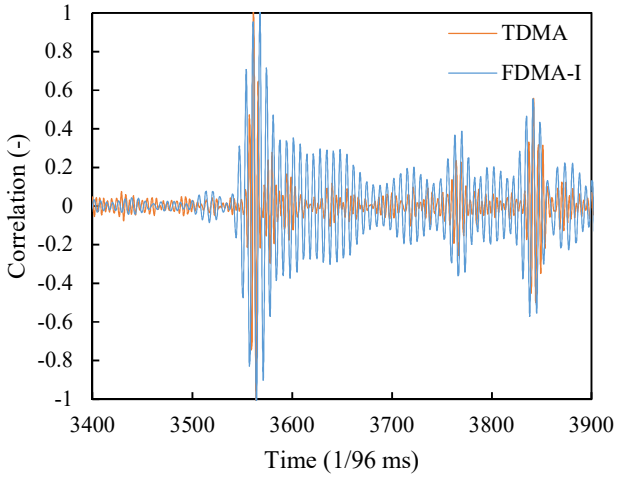


**Fig.4.7** Correlation result of FDMA-I signals and TDMA signals

As Fig.4.6 shows the 2D positioning error distribution of the four methods, the result was separated by less than 20 mm, from 20 mm to 50 mm, from 50 mm to 100 mm, and larger than 100 mm. Besides the low detection rate of FDMA, the overlapping problem is one of the reasons that increased the range error and contribute for the high position error in FDMA-II and FDMA-III (25% as well as 50% of the overlapping

frequency). Obviously TDMA is the best performed method in this static greenhouse setting, FDMA-I without overlapping frequency is the best among all the FDMA performances.

Fig.4.7 shows the correlation examples of FDMA-I and TDMA at position No.7, the SS Sound signal emitted from Speaker 1. Both FDMA-I and TDMA should give the same time of arrival which the peak was located at the signal sample of 3561, as the signal transmission distance was the same. FDMA-I signal has a larger peak width than the TDMA's signal that the large peak width which is determined by chip rate and carrier frequency. The large peak width will lead to a large tolerance for the true peak and reduce the accuracy of the distance calculation. Meanwhile, the threshold can identify the direct wave, which is the first received peak of the signal, from the reflected wave. As Fig.4.7 shows there was a clear peak in TDMA received signal, the chip rate of the TDMA signal is 12 kcps, M-sequence length is 1023, the length of the sub-peaks is 4 samples, each sample represents 1/96 ms, which is resulted from the signal generation. This peak width will result maximum 14 mm error in distance measurement for TDMA (Huang et al., 2020) and 52 mm error in FDMA-I.

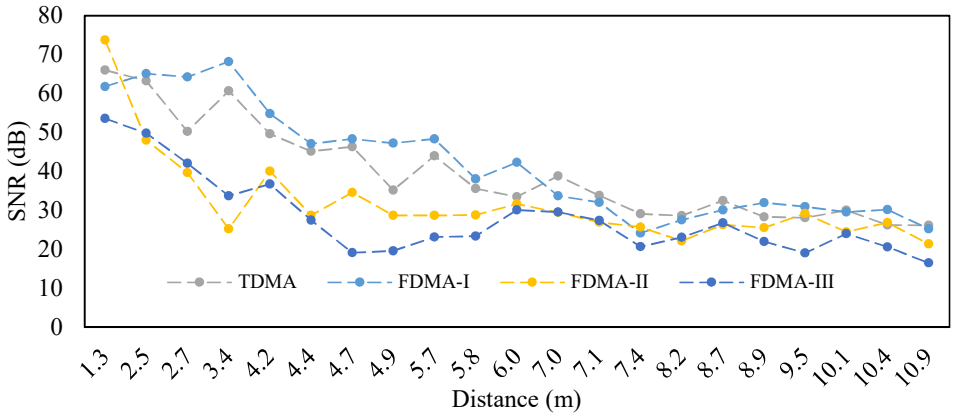


(a)

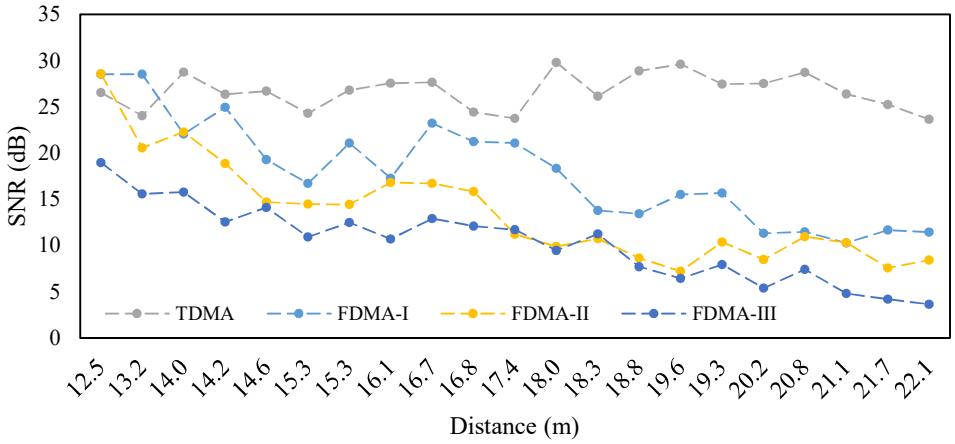


(b)

**Fig.4.8** Evaluation of TDMA and FDMA SNR at (a) Speaker 2 and (b) Speaker 4

Fig.4.8 illustrates relationship between carrier frequency and SNR against distance attenuation. The x-axis is the distance from the speakers to the target microphone. In Fig.4.8(a) shows the SNR results of Speaker 2 was located very close from the experiment points of microphones, therefore, the graph shows a similar result for attenuation effect. It is believed that the TDMA performed similar with FDMA-I methods because they share the same carrier frequency.

Fig4.8(b) shows the SNR from a long range of the signal transmission, x-axis is the distance from Speaker 4 to the target microphone. Because the experiment condition is set to make the worst situation for channel interference of speaker at a far distance with a speaker at a close distance. The strength of SS Sound, in respect to the noise, is described as the larger the SNR, the larger the noise tolerance. Normally, the arrival time of the sound signal is difficult to be detected when SNR value is small. The FDMA method does not show it competitive compare to TDMA especially for a long range. The reason is believed to be the interference of SS Sound signal as well as the attenuation of high frequency sound in air against distance which means the sound pressure level damps as distance increases, and the atomosphere absorption increases

as sound frequency elevates.

### 4.3.2 Dynamic positioning of TDMA and FDMA

**Table 4.3** Results of the dynamic results

| Signals | 2D error (mm) | Range error (mm) |
|---|---|---|
| TDMA | 180.3 ± 71.4 | 92.3 ± 34.5 |
| FDMA-I | 62.1 ± 22.5 | 41.5 ± 13.5 |

Table 4.3 shows the dynamic results of the TDMA and FDMA. The position error for TDMA is 180.3 ± 71.4 mm and the FDMA result is 62.1 ± 22.5 mm. The mean absolute range error of TDMA and FDMA are 92.3 ± 34.5 mm and 41.5 ± 13.5 mm respectively. Cultivation types have different accuracy requirements for a positioning system. For example, there are four planting modes for a strawberry greenhouse: table-top, bench-type, elevated-substrate, and ridge-planting (Yu et al., 2020), and the corresponding robot movable path widths are 100 cm, 80 cm, 60 cm, and 35 cm, respectively.

Assuming the robot width is 25 cm, the robot can know which furrow is running and its current location in a table-top, bench-type or elevated-substrate cultivation strawberry greenhouse with the accuracy of the current positioning system. On the other hand, suppose only the proposed positioning system is used to guide the robot's path in a ridge-planting greenhouse. In that case, the 2D positioning accuracy should reach 5 cm to prohibit the robot won't run on the ridge.

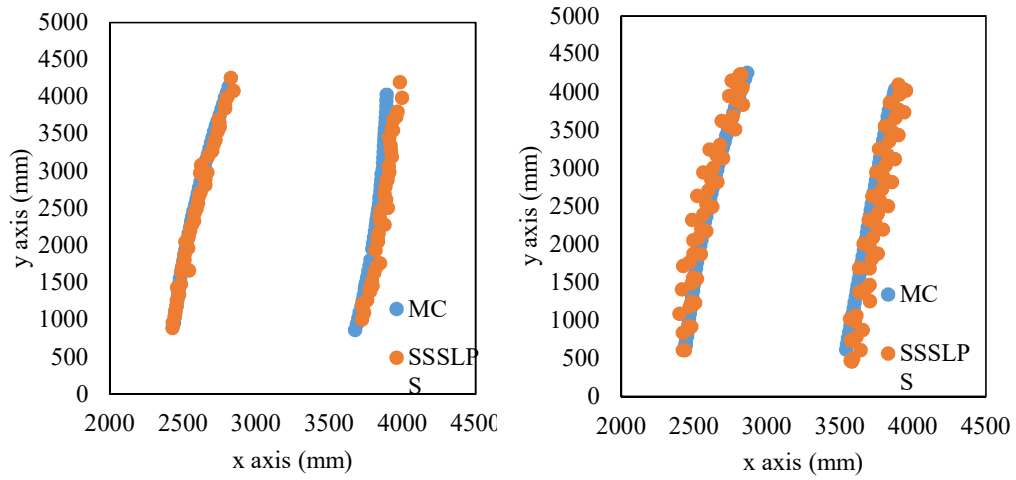


**Fig.4.9** Dynamic movement of (a) FDMA (b) TDMA

Fig.4.9(a) shows the trajectory of FDMA which is similar with the route of TDMA. The measurement of each method was performed four times independently and we can see that the FDMA position result of SSSLPS is much overlapped with Motion Capture references coordinates. The position error of the FDMA measurement results has a higher accuracy, that the average positioning error is 62.1 ± 22.5 mm. Fig.4.9(b) shows the measurements of TDMA that the SSSLPS coordinates have a shifting problem. TDMA time delay problem resulted in a shifting issue of the moving trajectory. It increased the error range as each speaker has an accumulative 250 ms delay for each speaker's measurement. For moving in a velocity of 300 mm/s, the average positioning error is 180.3 ± 71.4 mm. Concerning the TDMA time delay error with different velocity, we did a simulation from 100 mm/s to 1000 mm/s.

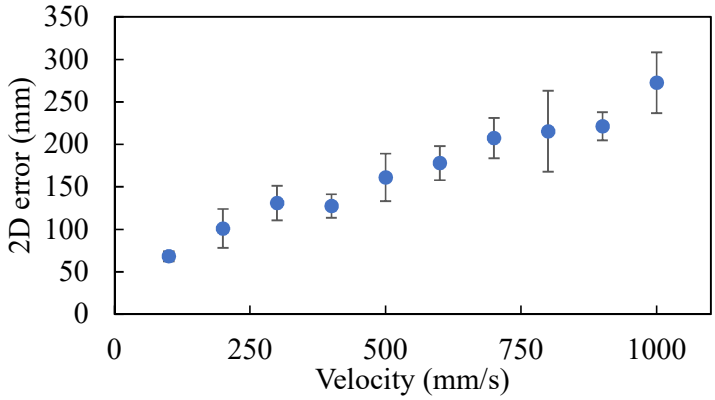


**Fig.4.10** TDMA simulation result of 2D position error with different moving speed

Fig.4.10 illustrates the TDMA simulation result of 2D position error versus the velocity of moving robot in a similar setting of the dynamic experiment environment. We can observe the simulation results that the time delay problem of TDMA will increase the positioning error. From the robot velocity of 100 mm/s, the position error is estimated at 68.2 ± 6.0 mm. When the moving speed is at 300 mm/s, the position error is anticipated to be 130.9 ± 20.2 mm assume ranging error was following a 25 mm Gaussian distribution. The simulation has excluded the frequency shifting problem and the Doppler shift algorithm for solving the frequency shifting in dynamic positioning. While we can anticipate that when the robot is moving at a higher speed, the position error will also increase according to the simulation model. It is possible to combine SSSLPS with other localization systems such as inertial measurement units as a hybrid system that our team simulated the improved localization results using the data from accelerometer and gyroscope (Tientadakul et al., 2020). Another possible approach to increase TDMA performance is increasing the update frequency by a shorter sound signal. However, this will worsen the noise tolerance of SS Sound.

## 4.4 Conclusions

To conclude, FDMA method suffered complex effects, including overlap signals

interference and high frequency sound damping whilst TDMA has an issue of the time delay for signal transmission. For static measurements, TDMA achieved an average 12.2 mm positioning accuracy in a greenhouse. Static experiment does not affect by the time delay problem but FDMA has a peak detection error which contributes the main error of positioning result and also high frequency damping problem. For the dynamic experiment, FDMA achieved an average 62.1 mm positioning accuracy. Since TDMA needs to allocate the time slots for each speaker, to measure a distance means the waiting time for a time slot is necessary.

It is obvious to see that the TDMA method has a time delay shifting problem, while FDMA method without frequency overlapping does not have such time delay problem and it is suitable to measure the position of moving agricultural robots. As the objective is to tackle the near-far problem of conventional SSSLPS, this study shows that TDMA method is suitable in static and slow-moving measurement, whilst FDMA method is suitable for measuring fast-moving robots.

# Chapter 5 Acoustic Based Local Positioning System for Dynamic UAV in GPS-denied Environment

## 5.1 Background

Recent greenhouse robotic systems are beginning to incorporate unmanned aerial vehicles (UAV) in order to perform various tasks more efficiently (Simon et al., 2018), such as measuring (Roldán et al., 2015) and mapping (Roldán et al., 2016) of greenhouse environmental variables, indoor livestock management (Krul et al., 2021), and yield estimation - tomato flower detection (Oppenheim et al., 2017). In the absence of UAV, most of these tasks are manually performed, which depends on the skills and availability of workers. In order to undertake relinquish such tasks to automated agricultural robotic systems, the positioning system (navigation) plays a crucial role guiding robotic motion. This is important in indoor environments, such as a greenhouse, where GPS based positioning systems are often unable to operate effectively.

We have already established, with a wire-linked system in a greenhouse, that a positioning system with a centimeter level accuracy and acoustic noise tolerance can be achieved over a 12 m × 6 m area (Huang et al., 2020). Other research has demonstrated the acoustic noise from a stationary quadcopter with a 9.7 N thrust increased the positioning error by 10 mm (Huang et al., 2020), while the movement of a low noise crawler robot can compensate a Doppler shift effect by the algorithm extracted the carrier wave (Huang et al., 2021). Now these two separate issues (noise and a Doppler shift effect) need to be simultaneously addressed, if a sound-based navigation system on board a dynamically moving UAV is to be used to perform machine vision analysis for the monitoring of plants in a greenhouse environment.

The objective of this research is to build a reliable low-cost and high accuracy positioning system for UAV to perform indoor plants monitoring and machine vision

system. We proposed a novel Doppler shift compensation algorithm which select the strongest correlation SNR signal from a series of correlation signals calculated using candidate Doppler shifted reference signals to obtain an accurate ToA. And, the dynamic positioning accuracy and measurement fail rate were evaluated in a closed indoor laboratory with using Motion Capture system as reference.

## 5.2 Materials and Methods

A wireless SSSLPS connected with the motion capture system was used for evaluating accuracy of the positioning system. The structure of the SSSLPS is shown in Fig.5.1. Four speakers (FT28D, Fostex) were connected to a PC though amplifiers (AP15d, Fostex) and an audio interface (OCTA-CAPTURE UA-1010, Roland) for converting analog signals to digital ones. The 3D printed cone shown in Fig.5.2(a) was mounted on the speakers to emit omnidirectional sound, which also enables the area of coverage to be enlarged. To prevent interference problem, the time division multiple access (TDMA) was applied. Therefore, each channels had a 250 ms time frame and period of emitting each channel SS Sound was 1 s (= 4 channels x 250 ms time frame).

Audio interface also output a trigger signal at the beginning of SS Sound time frame by using Zigbee device to obtain emitting time of SS Sound. The wireless SSSLPS receiving unit (Fig.5.2) consists of a Field Programmable Gate Array (FPGA) board, an integrated sensor board and a Jetson Nano processor, attaching two microphones (SPU0410LR5H-QB-7, Knowles Electronics, frequency response ± 3 dB) for recording the SS Sound signals, Zigbee device to receive trigger signal.

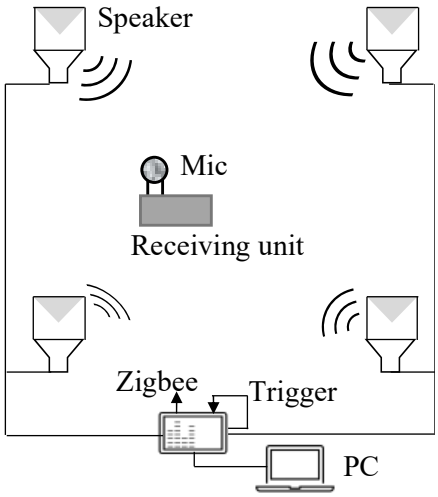


**Fig.5.1** Structure of the positioning system

(a)

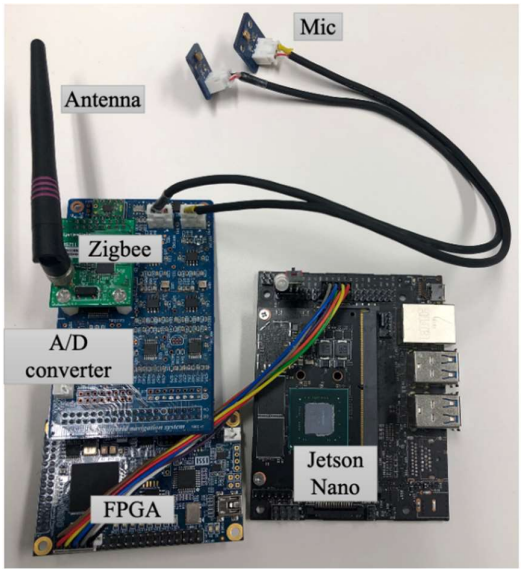


(b)

**Fig.5.2** (a) The speaker with a 3D printed cone and (b) hardware of the receiving unit

## 5.2.2 Doppler shift compensation

### 5.2.2.1 Previous compensation method

There mainly has two conventional Doppler shift compensation algorithms, one used an extra carrier wave to estimate the frequency shift (Widodo et al., 2013), which occupied the power spectrum and led to a lower sound pressure level of an emitted signal. The extra carrier wave method cannot be applied to the UAV localization at a noisy environment. Another compensation algorithm extracts the carrier wave by digital signal processing (Huang et al., 2021) (Fig.5.3). At first, the received signal *R(t)* was filtered by a bandpass filter (BPF), then the signal was shifted into low frequency by multiplying a sine wave. The low pass filter (LPF) cut high frequency noise. After that, $(.)^2$ is a square function for removing M-sequence signals, and carrier wave frequency was detected by fast Fourier transform (FFT). The Doppler shift was evaluated by the carrier wave. In this research, this extracted algorithm method was

used as previous method to compare proposed method.

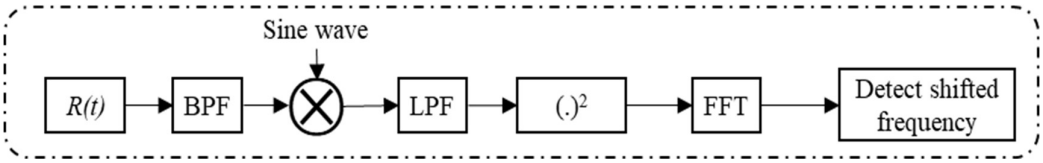


**Fig.5.3** Block diagram of conventional Doppler compensation by extracting the carrier wave

### 5.2.2.2 Proposed compensation algorithm

The proposed compensation algorithm uses an estimated frequency shift calculated from the setting UAV's moving velocity as the Doppler shift Eq.(11).

$$f_m = f_s \times \frac{v_s \pm v_r}{v_s}$$
$$\Delta f = f_m - f_s \tag{11}$$

where $f_m$ [Hz] is the observed frequency, $f_s$ [Hz] is the signal frequency, $v_r$ [m/s] is the predicted speed of the UAV viewed from the observer, $v_s$ [m/s] is the speed of sound. $\Delta f$ [Hz] is the estimated frequency shift, which would be a positive value if the source and observer are approaching each other, $\Delta f$ would be negative if the observer is receding from the source. Since the objective is to control a drone taking machine vision data at a moving speed of 200 mm/s, the resulting estimation of frequency shift would be ± 15 Hz, steps of 1 Hz. As a result, we choose to estimate the frequency shift from 23985 Hz to 24015 Hz.

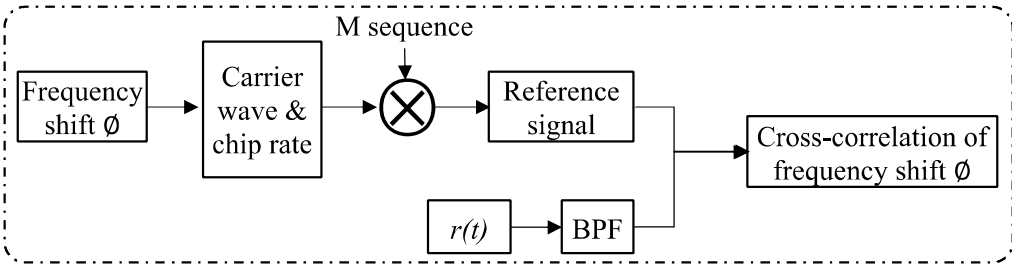


**Fig.5.4** Block diagram of calculating cross-correlation at frequency shift ∅

Fig.5.4 shows the proposed algorithm using estimating frequency shift ∅ and getting a new chip rate before performing the cross-correlation calculation. Every time a given frequency shift ∅ was used to generate the new carrier wave, which was multiplied with the updated M sequence chip rate for a new reference signal. This new reference signal at frequency shift ∅ was calculated for the cross-correlation. So totally 31 times cross-correlation were calculated. The correct signal has the highest signal strength that can be judged by the signal to noise ratio of correlation (SNR), as shown in the following Eq.(12).

$$\mathrm{SNR} = 20 \log \frac{C_p}{C_m} \tag{12}$$

where, $C_p$ is the maximum correlation value. $C_m$ is the mean value of correlation. Higher SNR value means higher signal strength against the noise. The algorithm will judge the highest SNR value as the correlation wave calculated by using the correct frequency shift.

## 5.3 Experiment

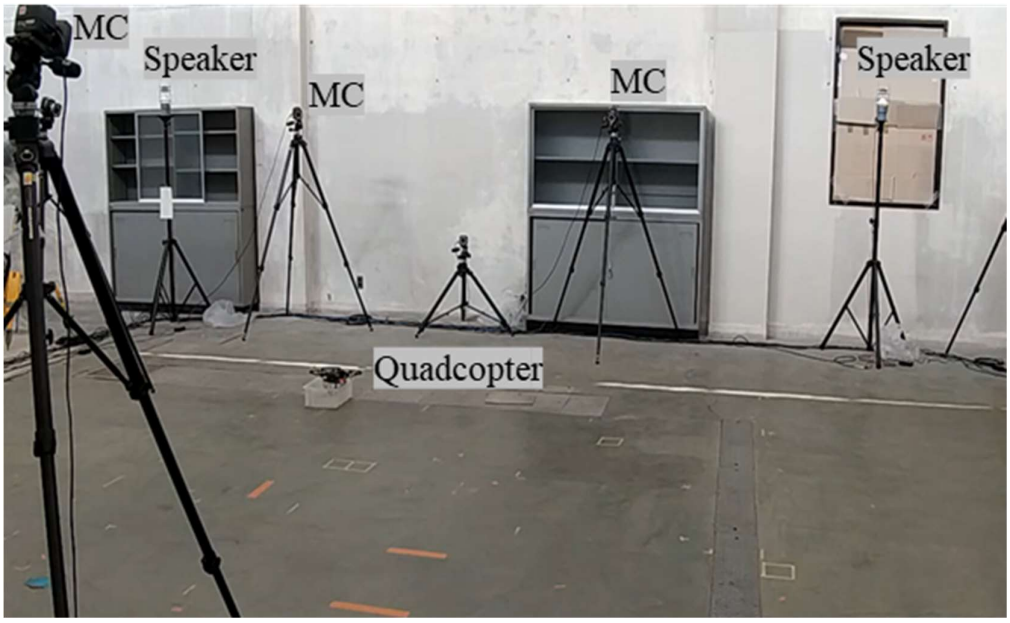


(a)

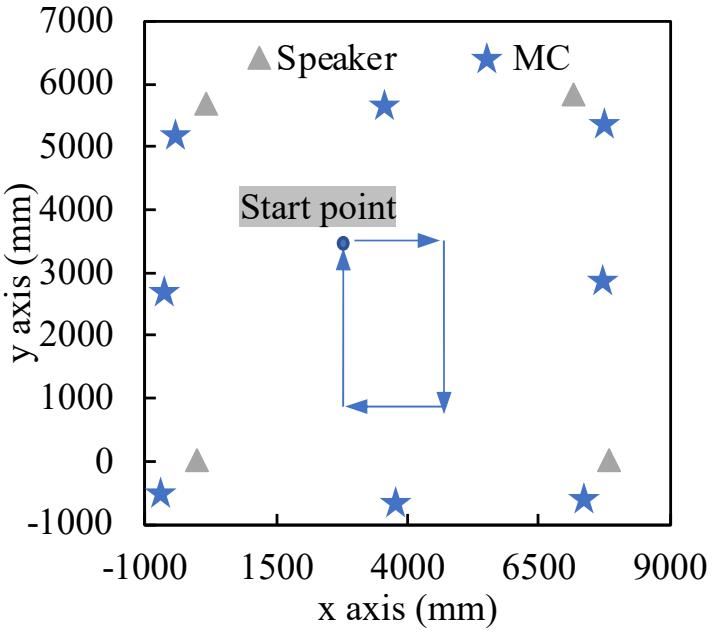


(b)

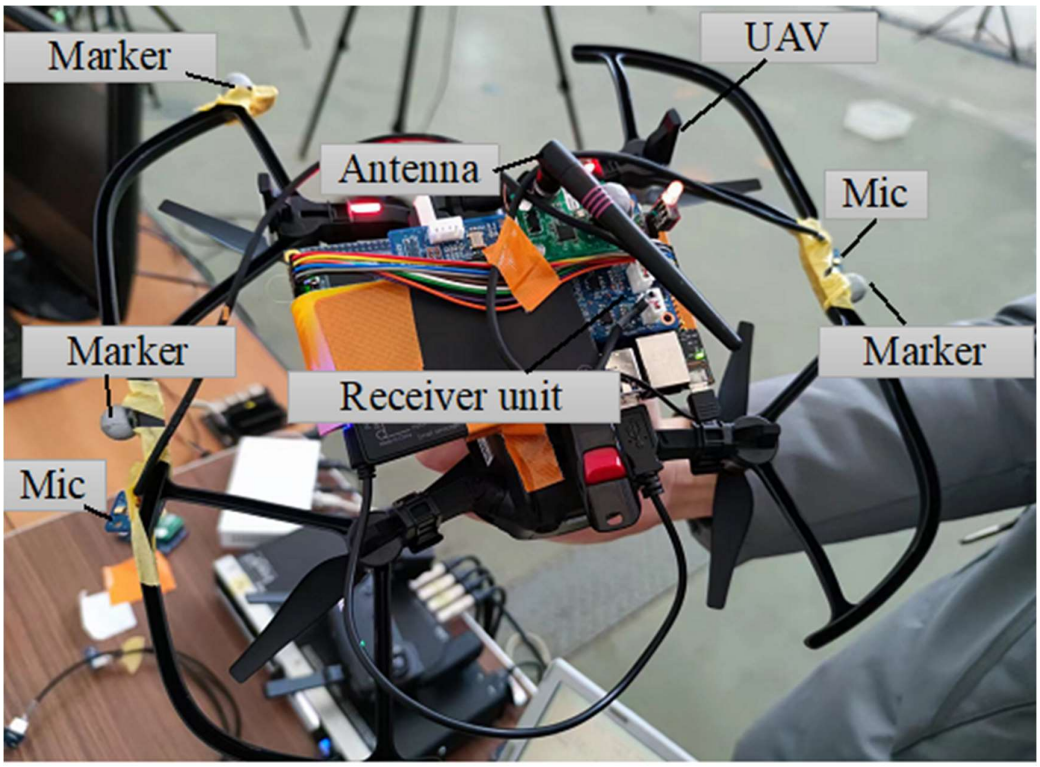


(c)

**Fig.5.5** Experimental (a) test field and (b) path plan (c) UAV

The experiment was conducted at Kyoto University on 17th February 2022. MC stands for motion capture cameras. The test field (Fig.5.5(a)) consists of 4 speakers and its height was set at around 200 mm above the ground. The sound pressure level of each speaker was set to 100 dB measured by a noise meter (LA-4440, Ono Sokki, frequency response ±1 dB). The 8-cameras Motion capture system (Vicon, Accuracy 0.1 mm) was also set in the field to evaluate SSSLPS positioning accuracy. Motion capture measured at 100 Hz and synchronized with SSSLPS using a trigger signal. A total station (Sokkia-SRX5XT32T-11, accuracy 1.5 + 2 ppm × measurement distance mm) was set outside the experimental area to calibrate the motion capture and SSSLPS coordinate. The calibrated coordinate had a maximum error of 1.5 mm.

We modified a UAV (Mavic Air, DJI) by putting the printed circuit boards under

the bottom part and attaching the microphones at the propeller guards next to the motion capture tracking markers (white dots) (Fig.5.5(c)). The moving path followed a rectangle size (Fig.5.5(b)). As for the experiment setting, we set the UAV speed of maneuvering at around 200 mm/s. This is because the objective of this project is monitoring plants with machine vision system. As the experimental room's doors and windows were closed, so there was no wind disturbance, and the temperature throughout the coverage area was relatively stable during the experiment at 20℃. Experiments were replicated 3 times to evaluate the performance of the proposed algorithm. In this experiment, microphones and trigger signals were just recorded by the Jetson Nano of the receiver unit. After taking the signals, we analyzed them using the PC.

### 5.3.1 Indoor UAV flight experiment

The position error of the proposed algorithm relative to the previous extracted algorithm method of are shown in Table 5.1. The distance will be recognized as failure measurement if the SNR value is smaller than 18 dB, determined from previous noise experiment results (Huang et al., 2020). Fail rate means the number of failure measurements over the total measurements. Without any compensation, the average positioning fail rate was 90%. Fail rate of the previous method was 27.9 % and much improved without any Doppler shift compensation. From this result, it found that a Doppler shift effect was large. The proposed algorithm has a better performance at a successful detection rate as the estimation of the frequency shift covers all the possible frequency shifts. The error of using the proposed algorithm was 74.5 ± 37.6 mm while using the previous method was 88.2 ± 60.2 mm. The positioning error of both methods were similar because the ToA calculation process is less affected by the proposed algorithm. However, the proposed algorithm can minimize positioning errors with a smaller standard deviation value. These results indicate that the algorithm has a better performance compared with the previous extracted algorithm method of Doppler

compensation that guarantees the system could be used for a dynamic robot. The reasons will be discussed in the following sections.

**Table 5.1** Fail rate and accuracy

| Method | Fail Rate | Max. Error | Min. Error | Mean Error | St. deviation |
|---|---|---|---|---|---|
| Previous method | 27.9% | 249.6 mm | 15.3 mm | 88.2 mm | 60.2mm |
| Spectrum Peak algorithm | 9. 8% | 206.3 mm | 18.6 mm | 74.5 mm | 37.6 mm |

Fig.5.6 is one example of measurement using the proposed system (SSSLPS) and the motion capture (MC) system. Manually controlling the quadcopter leads to the path having a vibration during movement. Four ranging measurement results were shown in Fig.5.7, and their corresponding means absolute errors were 86.1 mm, 81.1 mm, 92.3 mm, and 81.6 mm, separately. The mean absolute ranging error has the main effect on the positioning accuracy (Huang et al., 2021). In this experiment, the coverage area was about 8 m × 6 m, which was limited by the motion capture system. Previous research in a greenhouse using a static quadcopter with 9.75 N thrust shows the ability of SSSLPS for a 12 m × 6 m coverage (Huang et al., 2020). A typical solution for enlarging the coverage area is to use more speakers in the set up (Priyantha, 2005). Assuming a signal coverage for a SSSLPS on a quadcopter is 12 m × 6 m, adding more speakers could increase the coverage area.

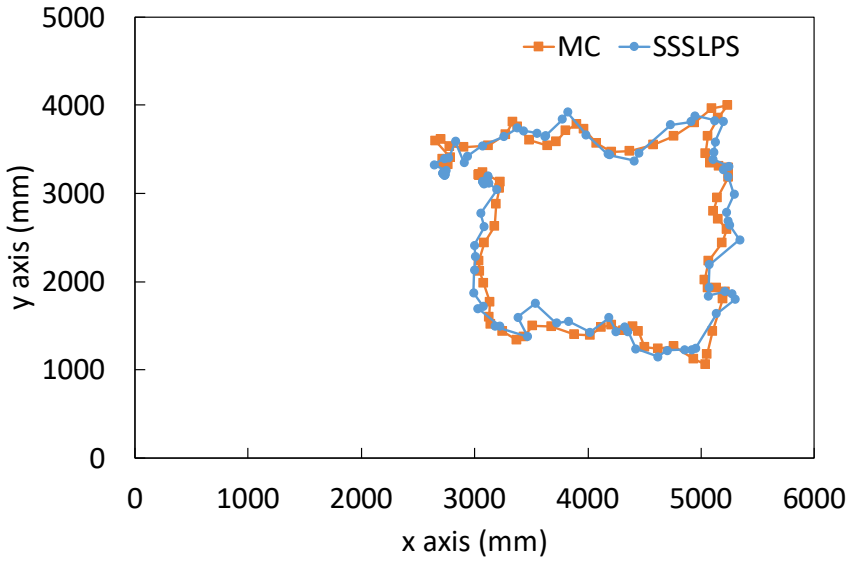


**Fig.5.6** 2D positioning measurement result

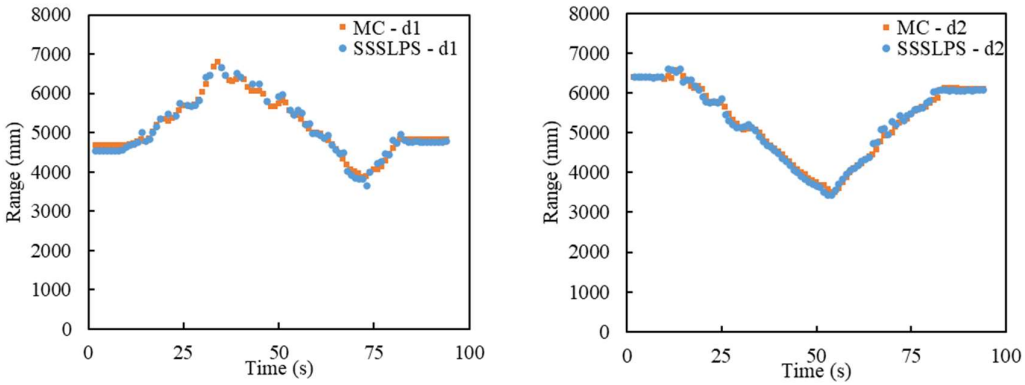


(a) (b)

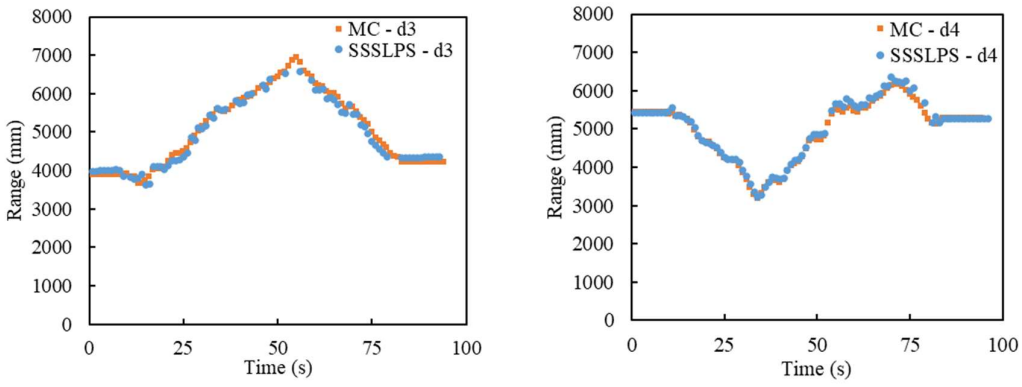


(c) (d)

**Fig.5.7** Ranging results of SSSLPS and motion capture from the microphone to (a) Speaker 1 (b) Speaker 2 (c) Speaker 3 (d) Speaker 4

### 5.3.2 Noise tolerance

As the SSSLPS is an acoustic-based system, the operation of the UAV creates propeller noise, as well as brushless motors noise issues over a wide bandwidth. A microphone (ECM-100N, Sony) with a frequency response from 0 to 48 kHz of ± 3 dB and a noise meter (LA-4440, Ono Sokki) with a frequency response in the hearing range of ± 1 dB were used to measure the acoustic noise spectrum of the quadcopter at the edge of the propeller, as reported in the previous research (Huang et al., 2020). The recorded the quadcopter noise, motor noise, and background environmental noise of our experiment are shown in Fig.5.8. Compare with the UGV's case that the noise was mainly distributed in a lower frequency range and would not affect the carrier frequency. Using previous method in a noisy surrounding environment, the interfered carrier frequency is causing difficulties in finding the correct signal correlation, thus the calculated ToA would be inaccurate. Whilst, the proposed method can tolerate the noise over a broad frequency spectrum can select a correct signal correction for calculating accurate ToA.

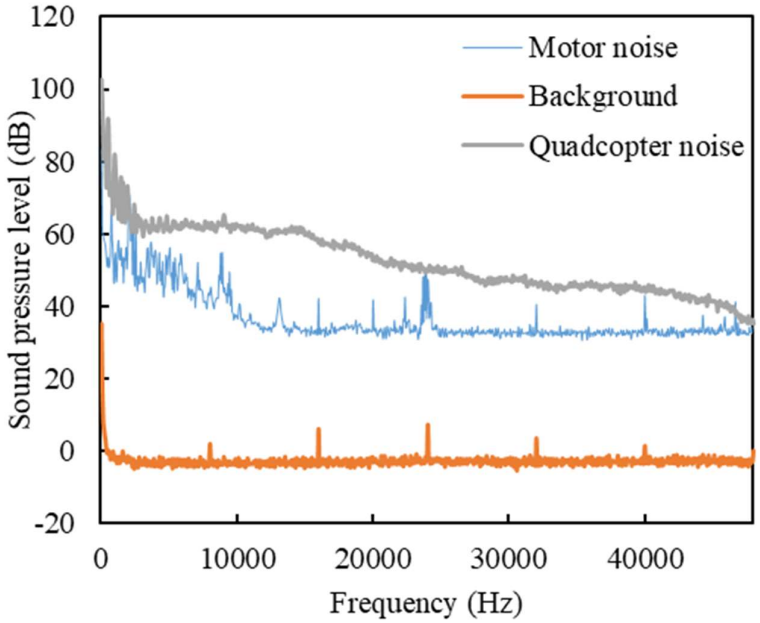


**Fig.5.8** Acoustic noise spectrum

Fig.5.9(a) is the successful frequency spectrum for Doppler shift estimation which can show the correct peak of frequency shift. On the contrary, Fig.5.9(b) is an example of the previous algorithm with a moving velocity of about 217.1 mm/s. Normally there should only have one peak in the frequency spectrum which is the carrier wave. With acoustic noise interference from a quadcopter, the carrier wave is difficult to be extracted, so the previous algorithm can't work well with a 27.9% positioning fail rate. The noise of the propeller and motor were distributed over a broad frequency range from around 83 dB and 64 dB in the same frequency range of SS Sound respectively. Since there were noise peaks around 24k Hz, selecting a different carrier frequency for the SSSLPS might be better in avoiding the UAV's noises.

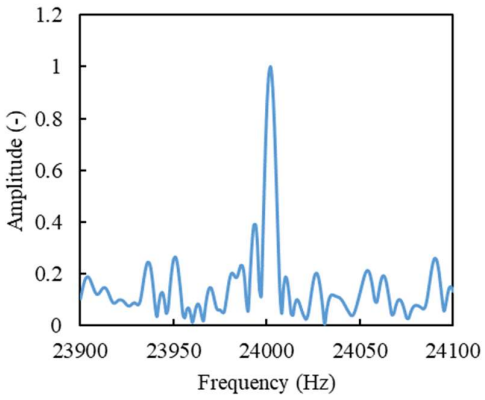


(a)

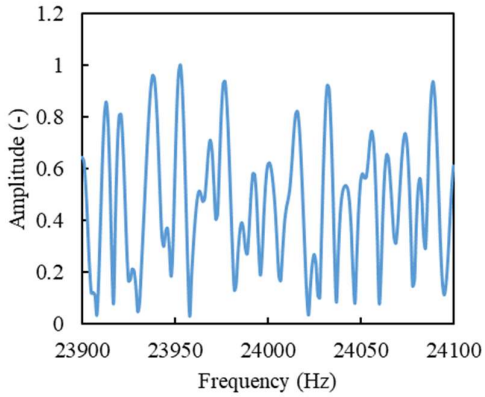


(b)

**Fig.5.9** Frequency spectrum examples of (a) successful case and (b) a failure case

### 5.3.3 Frequency steps optimization

As a comparison, the above signal was successfully processed by the proposed algorithm. Results of correlations are shown in Fig.5.10 that 24011 Hz is the selected correct spectrum shift. From 24010 Hz to 24012 Hz, the SNR are larger than 18 dB and for the other frequency shifts, the SNR are below 18 dB. To determine the optimal frequency steps of the algorithm, we can compare the computing costs and the fail rates

of frequency steps of 2 Hz and 3 Hz with 1 Hz. Comparing the CPU time processing the program with 1 Hz step, the process time of 3 Hz and 2 Hz steps would be 26.5% and 21.4% faster, however, they had a higher fail rate of 7.7% and 2.2% than that of 1 Hz respectively. Thus, a better frequency step is believed to be 2 Hz as balancing the computing cost and success rate of detection.

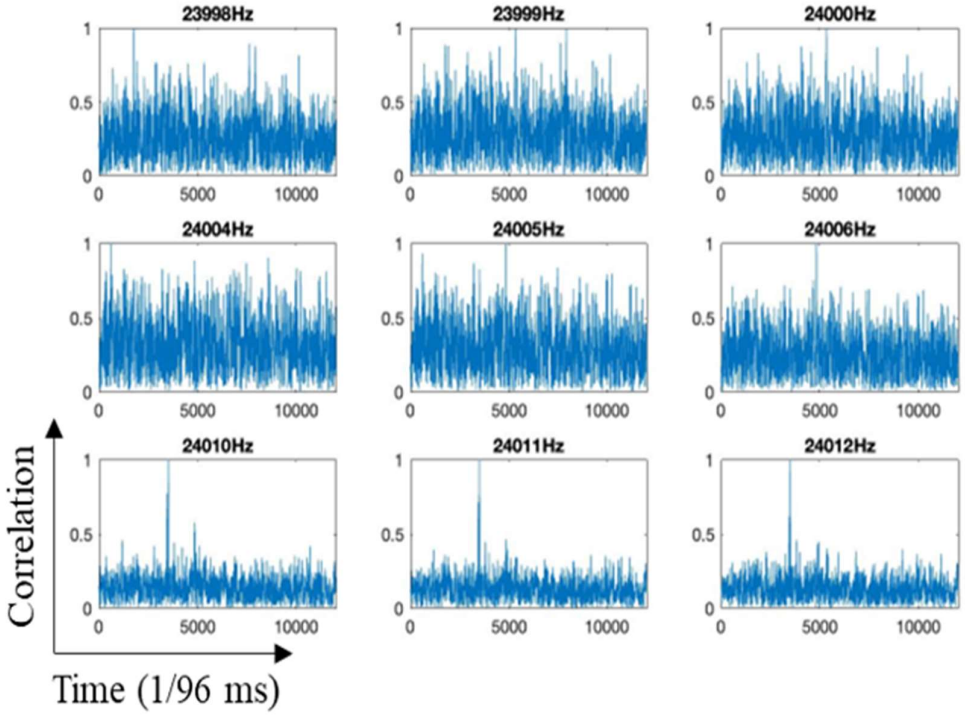


**Fig.5.10** Correlation at different frequency shifts

## 5.4 Velocity changes

The changing velocity during movement is another factor that can influence the Doppler shift compensation algorithm. The momentary (0.01 s) maximum and average moving velocities are 378.3 mm/s and 121.5 mm/s by calculating MC measurement data, separately. The previous and proposed algorithm assumes the velocity is constant

during movement (Huang et al., 2021; Widodo et al., 2013), however, in actual operation the UAV will not only generate noise interference, but will also have variations in velocity during movement. The average change of velocity during a signal length (0.171 s) was 49.1 mm/s$^2$.

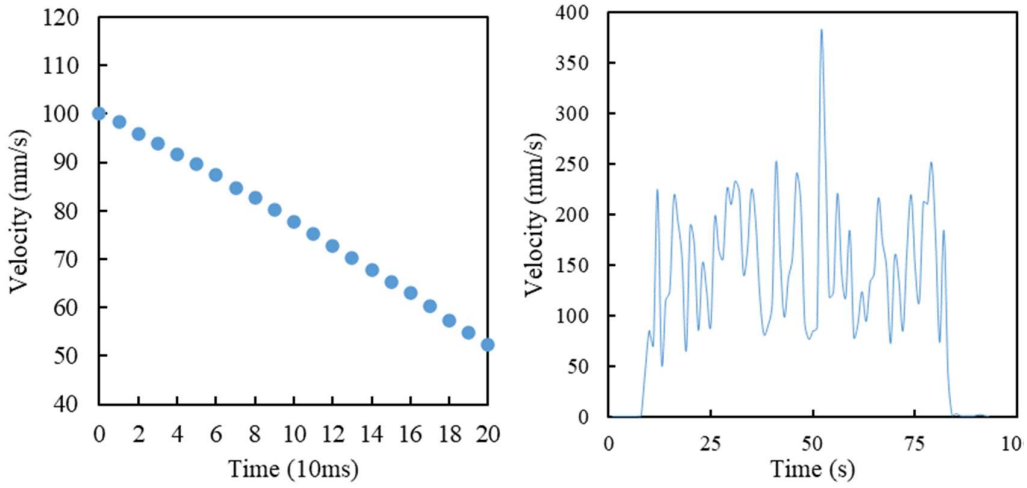


(a) (b)

**Fig.5.11** The velocity of UAV (a) within a signal transmission time and (b) the whole experiment

Fig.5.11 (a) shows an example of the moving speed has changed from 100 mm/s to 60 mm/s within a signal length. It shows that the UAV was decelerating during the distance measurement of the signal. During experiment, the UAV moving at a changeable velocity (Fig.5.11(b)). Comparing the UGV experiment result (Huang et al., 2021), the UGV moved at a constant velocity with the change of velocity during a signal length was less than 20 mm/s$^2$comparing to over 40 mm/s$^2$ of UAV's. This explains

that accuracy of UAV (74.5 mm) is worse than the UGV (50.3 mm) because of a larger velocity change of the UAV.

## 5.5 Conclusion

This research has shown that the proposed Doppler shift compensation algorithm can maximize the cross-correlation peak value of ToA estimation, getting the a more accurate positioning of the SSSLPS. By conducting indoor UAV experiments in an area of 8 m × 6 m, the results showed the proposed Doppler shift compensation algorithm reached an improved accuracy of 74.5 ± 37.6 mm and success rate of 90.2% compared to the previous method's accuracy of 88.2 ± 60.2 mm and success rate of 72.1%.

The results also discuss the frequency steps of 2 Hz in algorithm is better for successful detection rate and calculation cost. The disadvantage of the proposed algorithm is the demand for computing resources when estimating the frequency shift of each SS Sound signal. The overall results proved that SSSLPS using the proposed algorithm could be a suitable localization system to guide UAV working in indoor fields such as warehouses or greenhouses.

# Chapter 6 Conclusions and Future Plan

## 6.1 Conclusions of all chapters

The research proposed a novel acoustic-based localization system, SSSLPS, with the temperature compensation and signal co-channel interference tolerance for controlling UAV and UGV to operate in an indoor environment. The experiments from a small-sized greenhouse to a large-sized commercial greenhouse have demonstrated a centimeter accuracy of the SSSLPS in the practical situations and the followings are the main findings in this work.

**Chapter 2** introduces the structure of the SSSLPS using four speakers at the corner and microphones on the robot. A wireless GPS-liked SSSLPS with Zigbee for trigger synchronization can localize multiple targets with putting receiver unit on UGV or UAV. The position can be estimated using at least three distances from speakers to microphone and we can expand the coverage with adding more speakers.

**Chapter 3** proposed a novel temperature compensation algorithm using the linear equation and Taylor expansion. The estimated sound velocity can achieve a better accuracy (14 mm) compare with the temperature sensor method (30 mm) and can tolerate temperature variations up to 11 °C. Results indicate the proposed estimated method has a positioning accuracy to within 20 mm in a 3 m x 9 m ridged greenhouse. The temperature compensation algorithm can estimate the sound velocity of the SSSLPS without using any temperature sensors.

**Chapter 4** evaluates the co-channel interference of TDMA and FDMA in SSSLPS and compares their performance. FDMA method suffered complex effects, including overlap signals interference and high frequency sound damping whilst TDMA has an issue of the time delay for signal transmission. For the case of average SNR, FDMA

(9.57 dB) performed worse than TDMA (28 dB) did, in which the average accuracy of FDMA is 31.6 mm also worse than TDMA's 12.2 mm accuracy in the 8.3 m × 22 m greenhouse. To solve the signal co-channel interference problem, FDMA can be applied in fast moving robot with a high update rate, whilst TDMA has the advantages of large coverage area and high accuracy which is suitable for slow-moving UGV and UAV with a low updating frequency in the large commercial greenhouse.

**Chapter 5** develops the frequency shift algorithm solving the problem of UAV noise and Doppler shift with finding an accurate correlation peak. Compare with the previous method of using extracted carrier wave, the proposed algorithm of estimation of the frequency shift reduced the fail rate from 27.9% to 9.8%. The proposed algorithm has not only a better performance at a successful detection rate as the proposed algorithm covers all the possible frequency shifts, also improved the accuracy from 88.2 mm to 74.5 mm using the proposed algorithm.

The results show the research improved the SSSLPS from compensating the temperature error without using sensors, tolerating the signal co-channel interference and also extending the system to localize UAV using a new Doppler shift algorithm. This research fulfilled the objective of providing a low-cost and high accuracy acoustic localization system for unmanned robots with temperature and signal co-channel interference tolerance.

## 6.2 Future plan

The future work of this research is to enlarge the coverage area to a large-scale localization system. While developing a hybrid system with inertial measurement units (IMU) will be the next step to increase the robustness of the system, as well as improving the noise tolerance of the system. For the system structure, there are much

room for improving the processing time from either reducing the software codes or redesign the hardware circuit board.

The final goal of this research is to accomplish the SSSLPS and use it as the navigation for a fully automation in precision agriculture. In order to realize this goal, a compact design robot system is also included in the future tasks. It is believed that SSSLPS can be used in the presence of operating multiple robots in the challenging environments.

Concerning the future applications, the use of SSSLPS can be extended to aquaculture or under water localization and many other complicated environments due to the acoustic properties. The acoustic signals could penetrate through water and would not interfere with sensitive equipment that uses electromagnetic wave. SSSLPS has a tremendous potential for guiding robots and localizing any objects in different situations.

# References:

Aguilera, T., Alvarez, F.J., Sanchez, A., Albuquerque, D.F., Vieira, J.M.N., Lopes, S.I., 2015. Characterization of the Near-Far problem in a CDMA-based acoustic localization system, in: 2015 IEEE International Conference on Industrial Technology (ICIT). Presented at the 2015 IEEE International Conference on Industrial Technology (ICIT), IEEE, Seville, pp. 3404–3411. https://doi.org/10.1109/ICIT.2015.7125604

Atri Mandal, C.V.L., 2005a. Beep: 3D indoor positioning using audible sound, in: Second IEEE Consumer Communications and Networking Conference, 2005. CCNC. 2005. Presented at the Second IEEE Consumer Communications and Networking Conference, 2005. CCNC. 2005, IEEE, Las Vegas, NV, USA, pp. 348–353. https://doi.org/10.1109/CCNC.2005.1405195

Atri Mandal, C.V.L., 2005b. Beep: 3D indoor positioning using audible sound, in: Second IEEE Consumer Communications and Networking Conference, 2005. CCNC. 2005. Presented at the Second IEEE Consumer Communications and Networking Conference, 2005. CCNC. 2005, IEEE, Las Vegas, NV, USA, pp. 348–353. https://doi.org/10.1109/CCNC.2005.1405195

Bechar, A., Vigneault, C., 2016. Agricultural robots for field operations: Concepts and components. Biosystems Engineering 149, 94–111. https://doi.org/10.1016/j.biosystemseng.2016.06.014

Bellone, T., Dabove, P., Manzino, A.M., Taglioretti, C., 2016. Real-time monitoring for fast deformations using GNSS low-cost receivers. Geomatics, Natural Hazards and Risk 7, 458–470. https://doi.org/10.1080/19475705.2014.966867

Chan, E.C.L., Baciu, G., Mak, S.C., 2009. Using Wi-Fi Signal Strength to Localize

in Wireless Sensor Networks, in: 2009 WRI International Conference on Communications and Mobile Computing. Presented at the 2009 WRI International Conference on Communications and Mobile Computing (CMC), IEEE, Kunming, Yunnan, China, pp. 538–542. https://doi.org/10.1109/CMC.2009.233

De Preter, A., Anthonis, J., De Baerdemaeker, J., 2018. Development of a Robot for Harvesting Strawberries. IFAC-PapersOnLine 51, 14–19. https://doi.org/10.1016/j.ifacol.2018.08.054

Delamare, M., Boutteau, R., Savatier, X., Iriart, N., 2019. Evaluation of an UWB localization system in Static/Dynamic. Presented at the IEEE International Conference on Indoor Positioning and Indoor Navigation (IPIN), Pisa, Italy, p. 8.

Hayashi, S., Yamamoto, S., Saito, S., Ochiai, Y., Kamata, J., Kurita, M., Yamamoto, K., 2014. Field Operation of a Movable Strawberry-harvesting Robot using a Travel Platform. JARQ 48, 307–316. https://doi.org/10.6090/jarq.48.307

Huang, L., Zhang, S., Wang, J., Zhang, X., 2019. Classification of Improved Cross-Correlation Function to Determine Speaker Location from Microphone Array, in: 2019 IEEE Fifth International Conference on Big Data Computing Service and Applications (BigDataService). Presented at the 2019 IEEE Fifth International Conference on Big Data Computing Service and Applications (BigDataService), IEEE, Newark, CA, USA, pp. 209–214. https://doi.org/10.1109/BigDataService.2019.00036

Huang, Z., Jacky, T.L.W., Zhao, X., Fukuda, H., Shiigi, T., Nakanishi, H., Suzuki, T., Ogawa, Y., Kondo, N., 2020a. Position and orientation measurement system using spread spectrum sound for greenhouse robots. Biosystems Engineering 198, 50–62. https://doi.org/10.1016/j.biosystemseng.2020.07.006

Huang, Z., Jacky, T.L.W., Zhao, X., Fukuda, H., Shiigi, T., Nakanishi, H., Suzuki, T., Ogawa, Y., Kondo, N., 2020b. Position and orientation measurement system using spread spectrum sound for greenhouse robots. Biosystems Engineering 198, 50–62. https://doi.org/10.1016/j.biosystemseng.2020.07.006

Huang, Z., Shiigi, T., Tsay, L.W.J., Nakanishi, H., Suzuki, T., Ogawa, Y., Naoshi, K., 2021. A sound-based positioning system with centimeter accuracy for mobile robots in a greenhouse using frequency shift compensation. Computers and Electronics in Agriculture 187, 106235. https://doi.org/10.1016/j.compag.2021.106235

Huang, Z., Tsay, L.W.J., Shiigi, T., Zhao, X., Nakanishi, H., Suzuki, T., Ogawa, Y., Kondo, N., 2020c. A Noise Tolerant Spread Spectrum Sound-Based Local Positioning System for Operating a Quadcopter in a Greenhouse. Sensors 20, 1981. https://doi.org/doi.org/10.3390/s20071981

Huang, Z., Tsay, L.W.J., Shiigi, T., Zhao, X., Nakanishi, H., Suzuki, T., Ogawa, Y., Kondo, N., 2020d. A Noise Tolerant Spread Spectrum Sound-Based Local Positioning System for Operating a Quadcopter in a Greenhouse. Sensors 20, 1981. https://doi.org/doi.org/10.3390/s20071981

Huang, Z., Wai Jacky, T.L., Zhao, X., Shiigi, T., Nakanishi, H., Suzuki, T., Naoshi, K., 2019. Noise Tolerance Evaluation of Spread Spectrum Sound-based Positioning System for a Quadcopter in a Greenhouse. IFAC-PapersOnLine 52, 239–242. https://doi.org/10.1016/j.ifacol.2019.12.528

Intaratep, N., Alexander, W.N., Devenport, W.J., Grace, S.M., Dropkin, A., 2016. Experimental Study of Quadcopter Acoustics and Performance at Static Thrust Conditions, in: 22nd AIAA/CEAS Aeroacoustics Conference. Presented at the 22nd AIAA/CEAS Aeroacoustics Conference, American Institute of Aeronautics and

Astronautics, Lyon, France. https://doi.org/10.2514/6.2016-2873

Jia, L., Xue, B., Chen, S., Wu, H., Yang, X., Zhai, J., Zeng, Z., 2019. A High-Resolution Ultrasonic Ranging System Using Laser Sensing and a Cross-Correlation Method. Applied Sciences 9, 1483. https://doi.org/10.3390/app9071483

Kawamura, N., Namikawa, K., Fujimura, T., Ura, M., 1984. Study on Agricultural Robot (Part 1). Journal of the Japanese Society of Agricultural Machinery 46, 353–358. https://doi.org/10.11357/jsam1937.46.3_353

Khyam, Md.O., Ge, S.S., Li, X., Pickering, M.R., 2017. Highly Accurate Time-of-Flight Measurement Technique Based on Phase-Correlation for Ultrasonic Ranging. IEEE Sensors J. 17, 434–443. https://doi.org/10.1109/JSEN.2016.2631244

Koura, Y., Suzuki, H., Ogawa, K., Kamei, Y., Nakamura, M., 2001. GPS COMPASS: A Low Cost GPS Direction Sensor of Two Antenna Type. Presented at the Proceedings of the 14th International Technical Meeting of the Satellite Division of The Institute of Navigation, Salt Lake City, UT, pp. 2700–2707.

Krul, S., Pantos, C., Frangulea, M., Valente, J., 2021. Visual SLAM for Indoor Livestock and Farming Using a Small Drone with a Monocular Camera: A Feasibility Study. Drones 5, 41. https://doi.org/10.3390/drones5020041

Kumar, M., 2017. Experimental study on natural convection greenhouse drying of papad. J. energy South. Afr. 24, 37–43. https://doi.org/10.17159/2413-3051/2013/v24i4a3144

Le, T.-K., Ono, N., 2015. Reference-distance estimation approach for TDOA-based source and sensor localization, in: 2015 IEEE International Conference on

Acoustics, Speech and Signal Processing (ICASSP). Presented at the ICASSP 2015 - 2015 IEEE International Conference on Acoustics, Speech and Signal Processing (ICASSP), IEEE, South Brisbane, Queensland, Australia, pp. 2549–2553. https://doi.org/10.1109/ICASSP.2015.7178431

Le, T.-K., Ono, N., 2014. Numerical formulae for TOA-based microphone and source localization, in: 2014 14th International Workshop on Acoustic Signal Enhancement (IWAENC). Presented at the 2014 14th International Workshop on Acoustic Signal Enhancement (IWAENC), IEEE, Juan-les-Pins, pp. 178–182. https://doi.org/10.1109/IWAENC.2014.6954002

Li, G., Tang, L., Zhang, X., Dong, J., Xiao, M., 2018. Factors affecting greenhouse microclimate and its regulating techniques: A review. IOP Conf. Ser.: Earth Environ. Sci. 167, 012019. https://doi.org/10.1088/1755-1315/167/1/012019

Madhani, P.H., Axelrad, P., Krumvieda, K., Thomas, J., 2003. Application of successive interference cancellation to the GPS pseudolite near-far problem. IEEE Trans. Aerosp. Electron. Syst. 39, 481–488. https://doi.org/10.1109/TAES.2003.1207260

Matano, T., Tanaka, T., 2003. Inverse-GPS Positioning Using Carrier Phase. IEEJ Trans. EIS 123, 255–261. https://doi.org/10.1541/ieejeiss.123.255

Mautz, R., 2009. Overview of current indoor positioning systems. Geodesy and Cartography 35, 18–22. https://doi.org/10.3846/1392-1541.2009.35.18-22

Mazhar, F., Khan, M.G., Sällberg, B., 2017. Precise Indoor Positioning Using UWB: A Review of Methods, Algorithms and Implementations. Wireless Pers Commun 97, 4467–4491. https://doi.org/10.1007/s11277-017-4734-x

Medina, C., Segura, J., De la Torre, Á., 2013. Ultrasound Indoor Positioning System Based on a Low-Power Wireless Sensor Network Providing Sub-Centimeter Accuracy. Sensors 13, 3501–3526. https://doi.org/10.3390/s130303501

Mercado, D.A., Flores, G., Castillo, P., Escareno, J., Lozano, R., 2013. GPS/INS/optic flow data fusion for position and Velocity estimation, in: 2013 International Conference on Unmanned Aircraft Systems (ICUAS). Presented at the 2013 International Conference on Unmanned Aircraft Systems (ICUAS), IEEE, Atlanta, GA, USA, pp. 486–491. https://doi.org/10.1109/ICUAS.2013.6564724

Merriaux, P., Dupuis, Y., Boutteau, R., Vasseur, P., Savatier, X., 2017. A Study of Vicon System Positioning Performance. Sensors 17, 1591. https://doi.org/10.3390/s17071591

Mostafa, M.H., Chamaani, S., Sachs, J., 2020. Singular Spectrum Analysis-Based Algorithm for Vitality Monitoring Using M-Sequence UWB Sensor. IEEE Sensors J. 20, 4787–4802. https://doi.org/10.1109/JSEN.2019.2962721

Ni, D., Postolache, O.A., Mi, C., Zhong, M., Wang, Y., 2019. UWB Indoor Positioning Application Based on Kalman Filter and 3-D TOA Localization Algorithm, in: 2019 11th International Symposium on Advanced Topics in Electrical Engineering (ATEE). Presented at the 2019 11th International Symposium on Advanced Topics in Electrical Engineering (ATEE), IEEE, Bucharest, Romania, pp. 1–6. https://doi.org/10.1109/ATEE.2019.8724907

Nikookar, H., Prasad, R., 2009. Introduction to Ultra Wideband for Wireless Communications. Springer, Dordrecht.

Penney, T., 2016. Noise has a new safety formula. URL

https://www.linkedin.com/pulse/noise-over-8-long-hours-work-has-new-safety-formula-you-terry-penney (accessed 2.27.22).

Oppenheim, D., Edan, Y., Shani, G., 2017. Detecting Tomato Flowers in Greenhouses Using Computer Vision. International Journal of Computer, Electrical, Automation, Control and Information Engineering 11, 104–109. https://doi.org/doi.org/10.5281/zenodo.1128833

Osada, Y., Fujimoto, H., Miura, S., Sweeney, A., Kanazawa, T., Nakao, S., Sakai, S., Hildebrand, J.A., Chadwell, C.D., 2003. Estimation and correction for the effect of sound velocity variation on GPS/Acoustic seafloor positioning: An experiment off Hawaii Island. Earth Planet Sp 55, e17–e20. https://doi.org/10.1186/BF03352464

Perret, J.S., Al-Ismaili, A.M., Sablani, S.S., 2005. Humidification-dehumidification system in a greenhouse for sustainable crop production. Presented at the Ninth International Water Technology Conference, Sharm El-Sheikh, Egypt, pp. 849–862.

Priyantha, N.B., 2005. The Cricket Indoor Location System. Massachusetts Institute of Technology.

Rajendra, P., Kondo, N., Ninomiya, K., Kamata, J., Kurita, M., Shiigi, T., Hayashi, S., Yoshida, H., Kohno, Y., 2009. Machine Vision Algorithm for Robots to Harvest Strawberries in Tabletop Culture Greenhouses. Engineering in Agriculture, Environment and Food 2, 24–30. https://doi.org/10.1016/S1881-8366(09)80023-2

Rishabh, I., Kimber, D., Adcock, J., 2012. Indoor localization using controlled ambient sounds, in: 2012 International Conference on Indoor Positioning and Indoor Navigation (IPIN). Presented at the 2012 International Conference on Indoor

Positioning and Indoor Navigation (IPIN), IEEE, Sydney, Australia, pp. 1–10. https://doi.org/10.1109/IPIN.2012.6418905

Roldán, J., Garcia-Aunon, P., Garzón, M., de León, J., del Cerro, J., Barrientos, A., 2016. Heterogeneous Multi-Robot System for Mapping Environmental Variables of Greenhouses. Sensors 16, 1018. https://doi.org/10.3390/s16071018

Roldán, J., Joossen, G., Sanz, D., del Cerro, J., Barrientos, A., 2015. Mini-UAV Based Sensory System for Measuring Environmental Variables in Greenhouses. Sensors 15, 3334–3350. https://doi.org/10.3390/s150203334

Shirehjini, A.A.N., Yassine, A., Shirmohammadi, S., 2012. An RFID-Based Position and Orientation Measurement System for Mobile Objects in Intelligent Environments. IEEE Trans. Instrum. Meas. 61, 1664–1675. https://doi.org/10.1109/TIM.2011.2181912

Simon, J., Petkovic, I., Petkovic, D., Petkovic, Á., 2018. Navigation and Applicability of Hexa Rotor Drones in Greenhouse Environment. Teh. vjesn. 25. https://doi.org/10.17559/TV-20161109211133

Spachos, P., 2020. Towards a Low-Cost Precision Viticulture System Using Internet of Things Devices. IoT 1, 5–20. https://doi.org/10.3390/iot1010002

Spachos, P., Papapanagiotou, I., Plataniotis, K.N., 2018. Microlocation for Smart Buildings in the Era of the Internet of Things: A Survey of Technologies, Techniques, and Approaches. IEEE Signal Process. Mag. 35, 140–152. https://doi.org/10.1109/MSP.2018.2846804

Tientadakul, R., Nakanishi, H., Shiigi, T., Huang, Z., Tsay, L.W.J., Kondo, N.,

2020. Indoor Navigation System by Combining Ultrasonic Wave TOA and Inertial Measurement, in: 2020 59th Annual Conference of the Society of Instrument and Control Engineers of Japan (SICE). Presented at the 2020 59th Annual Conference of the Society of Instrument and Control Engineers of Japan (SICE), pp. 1690–1695.

Vougioukas, S.G., 2019. Agricultural Robotics. Annu. Rev. Control Robot. Auton. Syst. 2, 365–392. https://doi.org/10.1146/annurev-control-053018-023617

Wenzhou, S., 2019. Analysis of the Influence about Uncertain Sound Velocity on the Positioning of Seafloor Control Points. OFOAJ 9. https://doi.org/10.19080/OFOAJ.2019.09.555768

Widodo, S., 2013. Wind and Doppler Shift Compensation for Spread Spectrum Sound-based Positioning System (PhD dissertation). Kyoto University.

Widodo, S., Shiigi, T., Hayashi, N., Kikuchi, H., Yanagida, K., Nakatsuchi, Y., Ogawa, Y., Kondo, N., 2013. Moving Object Localization Using Sound-Based Positioning System with Doppler Shift Compensation. Robotics 2, 36–53. https://doi.org/10.3390/robotics2020036

Yan, H., Chu, J., 2020. RFID Positioning Algorithm Based on BA Optimization, in: 2020 5th International Conference on Computer and Communication Systems (ICCCS). Presented at the 2020 5th International Conference on Computer and Communication Systems (ICCCS), IEEE, Shanghai, China, pp. 854–858. https://doi.org/10.1109/ICCCS49078.2020.9118539

Yang, X., Short, T.H., Fox, R.D., Bauerle, W.L., 1990. Transpiration, leaf temperature and stomatal resistance of a greenhouse cucumber crop. Agricultural and Forest Meteorology 51, 197–209. https://doi.org/10.1016/0168-1923(90)90108-I

Yu, Y., Zhang, K., Liu, H., Yang, L., Zhang, D., 2020. Real-Time Visual Localization of the Picking Points for a Ridge-Planting Strawberry Harvesting Robot. IEEE Access 8, 116556–116568. https://doi.org/10.1109/ACCESS.2020.3003034

## Acknowledgements

I would like to acknowledge many people for their guidance and support throughout my PhD study.

Firstly, I would like to express my sincere gratitude to my supervisor Prof. Naoshi Kondo, giving the academic advices and supervision during my time in Japan. Prof. Kondo always enlighten me with new stories and discuss the novel ideas with other researchers as well as businessmen.

I would like to thank Prof. Yuichi Ogawa and Prof. Tetsuhito Suzuki for their valuable comments, suggestions, and encouragement to my research. I would like to thank for their suggestions and comments. Prof. Garry J. Pillar helped me to proofread the abstracts and manuscripts.

I also would like to thank and give credits to Prof. Tomoo Shiigi from National Fisheries University and my buddy Dr. Zichen Huang for their helps and suggestions for my research, and guiding my experiment. I sincerely appreciate their enormous contribution to my research, especially the team discussion every week. Also, I would like to thank my former team members' suggestions about my research and assistant to my experiment.

It's my great honor to get the AFSLP for Master degree as well as the JST program for Doctoral degree at Kyoto University. This research was also supported by Japan Society for the Promotion of Science (JSPS) [Grant Number KAKENHI 18H05364], Japan Science and Technology Agency (JST SPRING) [Grant Number JPMJSP2110]. I would like to thank the Japanese Society of Agricultural Machinery and Food Engineers (JSAM) gave me the financial support to attend the CIOSTA & CIGR Section V Conference in Greece.

Last but not least, my family members supported me throughout the whole 20 years of academic studying. I sincerely thank my parent, Mr. Michael Tsay and Mrs. Helen Tsay, for their endless love and support. I would also thank my aunt Mrs. Jenny Ono, uncle Mr. Satoshi Ono for taking care of me in Japan.

Wish the COVID-19 could end soon; Hope there would be no war in the world.

Jacky Tsay

May 2022